Original Research Paper

IJES *Iranian Journal of Earth Sciences*
Vol. 15, No. 4, 2023, 228-247.
DOI: 10.30495/ijes.2023.1956689.1746

Geochemistry and tectonomagmatic environment of Eocene volcanic rocks in the Southeastern region of Abhar, NW Iran

Masoud Nazari[1], Mohammad Ali Arian[*1], Ali Solgi[2], Reza Zarei Sahamiyeh[3], Abdollah Yazdi[4]

1. Department of Geology, North Tehran Branch, Islamic Azad University, Tehran, Iran
2. Department of Geology, Science and Research Branch, Islamic Azad University, Tehran, Iran
3. Department of Geology, Lorestan University, Khorramabad, Iran
4. Department of Geology, Kahnooj Branch, Islamic Azad University, Kahnooj, Iran

Received 24 April 2022; accepted 2 October 2022

Abstract

Eocene volcanic are exposed in southeast of Zanjan in the Tarom magmatic zone that located in the Central Iran structural zone. The Abhar Eosen pyroclastic with andesite, trachy-andesite, dacite and rhyolite along with tuff compositions is located 120 km southeast of Zanjan. Mineralogically point of view, the studied volcanic rocks have low quartz, negligible alkaline feldspar, abundant plagioclase, and pyroxene contents. Textureally, Porphyritic, microlithic porphyritic, glomeroporphyritic, and poikilitic are predominant in these rocks. All of the studied samples display REE patterns characterized by LREE-enriched (Rb and Ba) and HREE-depleted segments typical of arc lavas which is one of the characteristics of subduction zone. The geochemical characteristics of the studied samples indicated that fractional crystallization is the primary cause of the diversity and differentiation of these rocks compared to crustal contamination. The rocks of the study area are composed of a similar origin to the OIB (mantle components) and partial melting of subcontinental lithospheric mantles. Of course, this mantle source has been modified by recycled sediments and melt released from the edge of the subducting oceanic crust.

Keywords: *Volcanic rocks; Active continental margin; Zanjan; Iran*

1. Introduction

Outcropped rock units in the Zanjan quadrangle map, from old to new, include Precambrian to Quaternary sequences, but volcanic rocks in this vast area are Eocene and younger. The most abundant volcanic rocks in this area are seen near Chenasvand, Changor, Hossein Abad, and Jurun Dagh villages. The Alborz Cenozoic magmatic activity, which is mostly of Paleogene age, is equivalent to the Karaj Formation in terms of stratigraphic divisions (Stocklin 1968; Annells et al. 1975). Zarei Sahamieh et al. (1992) have reported nummulite fossils in volcanic rocks in the north of Abhar. Eocene volcanic and pyroclastic rocks are outcropped as a gentle syncline with a northwest-southeast axis. In the simplified tectonic map of Iran-Turkey (Asiabanha and Foden 2012), the position of the Tarom magmatic zone in the structural zones of northern Iran and the study area is specified (Fig 1).

Researchers have no consensus on the origin and tectonic environment of the Cenozoic igneous eruptions in Tarom and, generally, in Iran. The research on the southern slopes of the Tarem Mountains can be summarized as follows: Ebrahimi et al. 2015 in the Aghkand range, Khademian et al. 2018 in the Amand range, Khalatbari Jafari et al. 2016, Esmaili et al. 2018 in Khalifelou (northern Abhar, Zanjan), Nadri and Aghazadeh in the Zaker-Sorkh Dizaj range, and Sadri Espushani et al. 2014 proved that the igneous complexes of the southern and southwestern slopes of Tarem had erupted in a magmatic arc of the active continental margin affected by subduction zones. According to these authors, these rocks have calc-alkaline to shoshonite metaluminous characteristics.

According to Seyed Qaraini et al. 2019, information obtained from field studies, lithology, geochemistry, and tectonic environment diagrams suggests that the intrusive masses of the Zajkan region are related to an enriched subduction-related lithospheric mantle and probably in a post-collision setting.

In another study, Khalatbari Jafari et al. (2016) investigated the petrography and geochemistry of the igneous rocks of the Agh-Dagh region in the north-eastern Abhar region, which are the eruptions of the Kurdkand unit. The results showed that the volcanic eruptions of the Aghdagh region have occurred during five phases in an offshore-onshore environment. These eruptions resulted in basic-intermediate and acidic volcanic deposits with a basaltic composition, including andesite, andesite, trachy-andesite, trachyte-trachy-dacite, dacite, and rhyolitic rocks. In the Agh Dagh region (Khalatbari Jafari et al. 2015), located on the southern side of the Tarem mountains, intermediate and acidic volcanic units have a larger expansion than basic units. These outcrops have a northwest-southeast trend and are folded in the form of thrusts and anticlines. Based on the paleontological investigation, microfossils

*Corresponding author.
E-mail address (es): maa1361@yahoo.com

from the middle-late Eocene age have been identified in the micrite limestones within the volcanic-sedimentary series. This evidence shows that the volcanic activities in the Aghdagh region took place during the middle-upper Eocene. Volcanic activities in this area have initiated with the eruption of rhyolitic-dacite lavas, which were repeated sequentially and upward with intermediate basic lavas. In the Aghdagh area, evidence of hybrid fractures and magmatic mixing can also be found in horizons with intermediate and acidic lavas. Based on thin section studies, these rocks show magmatic mixing and mixing, including the presence of basic-intermediate fragments in the acid paste, plagioclase with sieve texture, honeycomb structure, fluctuating zoning, and dissolved margin. These lavas contain large amounts of K_2O and have calc-alkaline, high-potassium calc-alkaline, and shoshonite magmatic compositions. The magmatic differentiation in this area can be attributed to three magmatic processes, from basic to acidic rocks. The intrusive masses of the Aghdagh region (Khalatbari Jafari et al. 2016; Khademian et al. 2018) are part of the type-I active continental margins and belong to the hybrid type of magmatic arc of the active continental margin. According to (Berberian and King 1981) and (MoinVaziri 1985), Cenozoic igneous eruptions in Iran are due to the subduction of Neotethys below Central Iran and the collision of the Iranian and Arabian micro-continent. (Alavi 1994) has considered the West Alborz-Azerbaijan magmatic band as a magmatic arc of the active continental margin due to the subduction of Neotethys under the Alborz micro-continent. Some researchers (Moayed 1991; Khalatbari Jafari et al. 2016; Dabiri et al. 2018) attribute the formation of Eocene volcanic rocks in the Alborz and Tarom region to the subduction phenomenon. In contrast, others have attributed the cause of Cenozoic magmatism in Iran to the presence of thermal blades beneath the Iranian block, similar to East Africa. They have been closed since the formation of the ocean (Sabzehei 1974; Emami and Ashja Ardalan 2005). Some researchers propose a back-arc tensile environment for the Alborz area in the Eocene (Hakimi et al. 2011; Hakimi and Bagherian 2018). For instance, (Didon and Gemain 1976), studying in Azerbaijan and Tarom regions, indicated the existence of a continental rift in the region. Meanwhile, a transtensional arc setting is proposed for some parts of the Tertiary volcanism in the Zagros orogen (Ebrahimi et al. 2017; Mehmood et al. 2023). According to Lescuyer & Riou (1976), the nature of Iranian magmas in the Cenozoic is not similar to continental rift and subduction zones and shows hybrid characteristics. Also, (Haghnazar and Malakotian 2013) and (Haghnazar and Shafei 2014) believe that the origin of Cenozoic volcanic rocks in Alborz is an oblique mantle source with spinel facies contaminated with continental crustal rocks, falsely showing the characteristics of subduction zones.

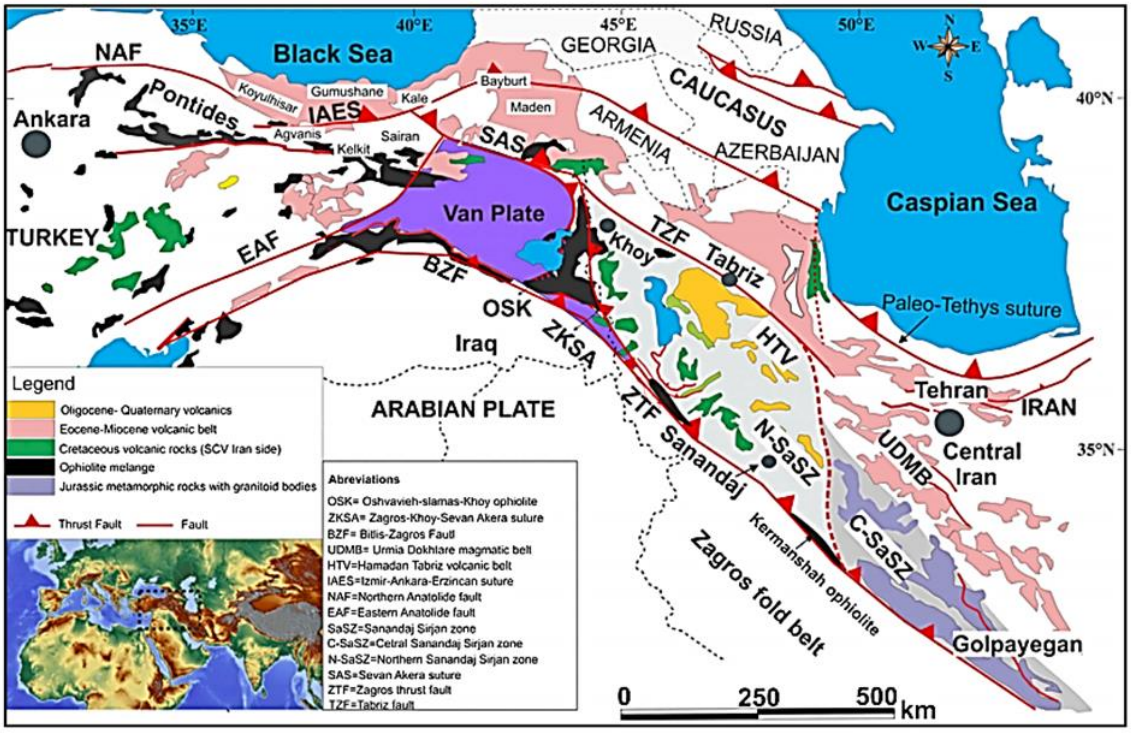

Fig 1. Distribution of the main suture zones and magmatic rocks from the Cretaceous to Quaternary in Turkey and northwestern Iran with the Van-microplate position. (Modified from Nouri et al. 2016).

2. Geology of the study area

The study area includes the southeast of the 1:100000 Abhar map, located 120 km southeast of Zanjan and south of the Tehran-Tabriz freeway. This area has coordinates of 49° 25′ to 49° 28′ E and 36° 05′ to 36° 15′ E and covers an area of 25 km^2. Geologically, it belongs to the Zanjan quadrangle. Also, according to Iran's geological and structural divisions by (Stocklin 1968) and (Nabavi 1976), it is part of Central Iran and the Western Alborz, respectively. According to (Hirayama et al. 1966), the volcanic and volcanoclastic complex in the northern quadrangle of Zanjan is comparable to the Karaj Formation regarding the lithostratigraphic affinity between them. Also, from the lithostratigraphic view, the rock units of the region are divided into two separate parts: i) pyroclastic of Karaj Formation and ii) plutonic and subvolcanic masses (Fig 2).

Volcanic rocks mainly include rhyodacite, dacite, intermediate acidic lavas (e.g., trachyandesite, andesite, and basaltic andesite), sand tuffs, lapilli tuffs, and breccia. Paleogene volcanic rocks are very thick and have mainly formed during three volcanic phases. The first phase includes submarine storms with sediments from the Eocene age (Karaj Formation) and is divided into two Kordkand and Amand members. Kordkand member starts with alternation of sandstone and mudstone tuff and ends with mudstone. On the other hand, the Amand member begins with a small tuff sandstone and ends with a tuff mudstone, along with lava-tuff alternations (Fig 3).

In the study area, in addition to volcanic rocks of the Karaj Formation, some intrusive massifs, dikes (especially doleritic dikes), and semi-deep intrusive massifs are also seen. Field visits of this area have shown that only three Ea. 4, Ea. 5, and Ea. 6 members of the Karaj Formation belong to the Amand complex (Hirayama et al. 1966), which are of Eocene age (Fig 2). Tertiary volcanic rocks cover older formations. The effect of intrusive massifs younger than Eocene on the surrounding rocks is so weak that it does not cause mineralization but causes the tuffs to become recrystallized. This behavior is probably due to the embedment of intrusive massifs at shallow depths. The units of Amand members observed in the study area have been merged due to their high similarity (Hirayama et al. 1966). In this respect, in the 1:50,000 map of Zanjan, units d, e, and f are called Ea4, g, h, i as Ea5, and unit j as Ea6. Quaternary in this area includes old disturbed terrace deposits (Q_1t) and talus or rock fragments (Qta) existing as rocks and pebbles in the rock slopes (Fig 2).

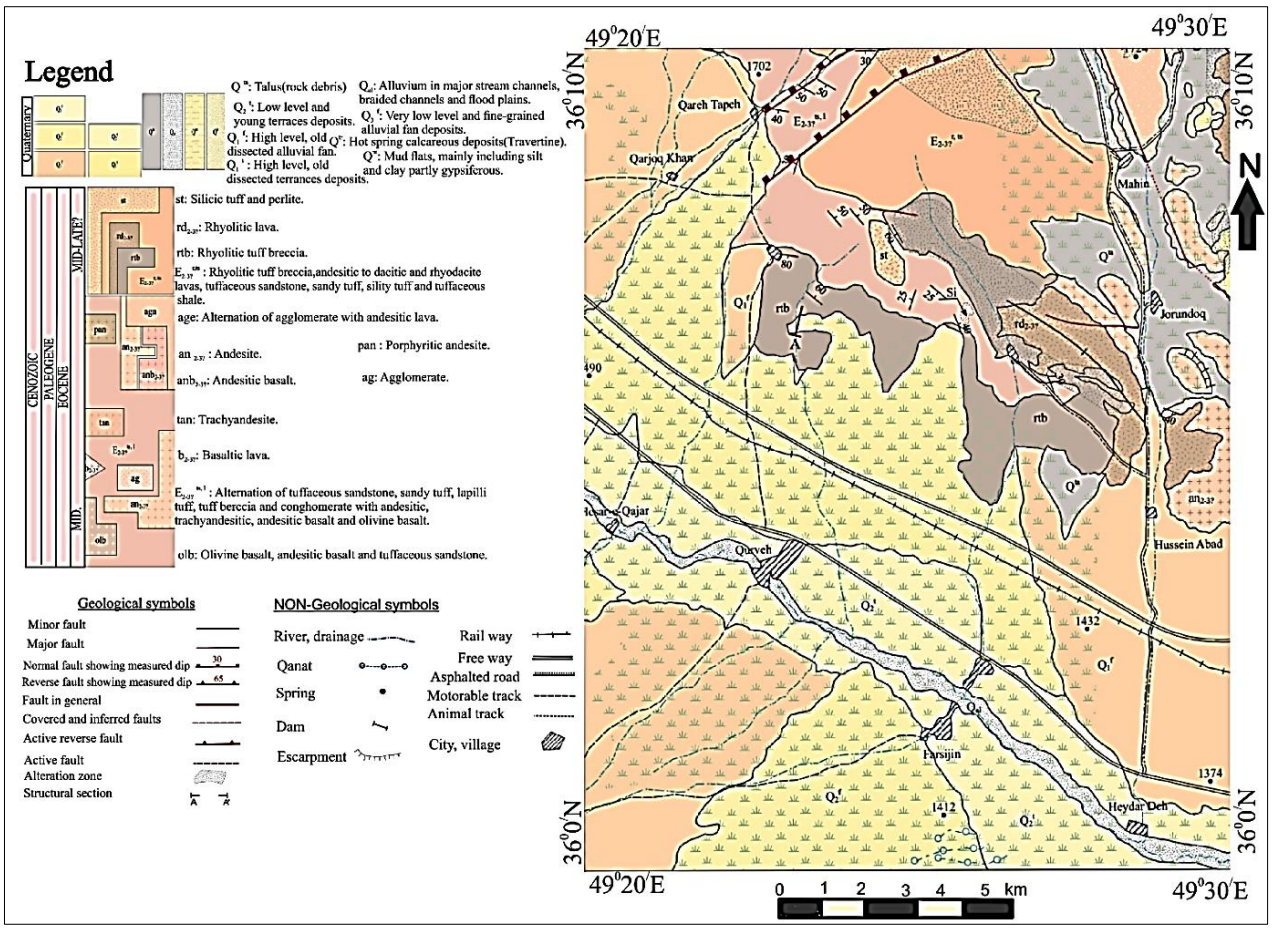

Fig 2. Geological map of the Abhar area (Hosseini Abhithabadi 1984).

Fig 3. Field photographs showing of the volcanic rocks of the study area.

3. Study method

During field operations, 50 samples were taken in systematic sampling, of which 30 thin sections were prepared. The samples were among the fresh outcrops and the weathered rims of the samples were removed before packing in plastic sample bags. And were studied by using Zeiss polarizing microscope in the Islamic Azad University, Science and Research Branch, Tehran. Next, the amounts of major, accessory, and trace elements were determined in the samples by analyzing 20 whole-rock samples through inductively coupled plasma mass spectrometry (ICP-MS) in Zarazma Company of Iran.

4. Lithography

Based on the lithographic studies performed on the samples of the study area, volcanic rocks of this area include andesite, trachyandesite, trachyte, dacite, andesitic tuff, trachyte-trachyandesite tuff, rhyodacite-dacite tuff, and rhyodacite tuff.

4.1. Trachyandesite

They appear in a dark grayish color with fine crystals or even without crystals. Plagioclases show polysynthetic twinning. These minerals have decomposed at the surface into calcite, chlorite, albite, and epidote. Based on the extinction angle, the measured plagioclageses are oligoclase-andesine (An_{28-34}). Also, they make up 30 to 35 vol.% of the rock matrix. Some plagioclases are degraded from the center to the outside and show a zoning structure. Alkaline feldspar is often subhedral and is of the sanidine type with the Carlsbad twinning. This mineral makes up 5 vol.% of the rock in cross-section. Biotite crystals are often anhedral to subhedral with a straight extinction. They have inclusions from other minerals such as opaque or iron oxides. This mineral makes up about 5 vol.% of the rock in cross-section. Pyroxenes are found in microcrystalline sizes. They are of the augite type and are mostly decomposed into auralite amphiboles, making 5 vol.% of the rock in thin section. Iron oxides or opaques are the accessory minerals of these rocks. Secondary minerals of this rock are calcite, chlorite, epidote, and iron oxides, which have been generated due to the decomposition of plagioclase and mafic minerals (Fig 4a).

4.2. Andesite

They appear in macroscopic scale or hand samples in gray to grayish pink colors. Under the microscope, this rock consists of plagioclase and pyroxene phenocrysts embedded in a microcrystalline matrix. They have porphyritic and glomeroporphyritic textures. Plagioclase minerals are seen in anhedral, subhedral, and euhedral forms and indicate polysynthetic twinning and even

zoning structures. The extinction angle measurements (An_{48-50}) show that they are of andesine type. Plagioclases make up 35 to 40 vol.% of the rock in thin section. Pyroxene crystals appear orange to pink under the polarized light. They are often subhedral and fine to medium crystals. These minerals make up about 10 vol.% of the rock in the thin section. Tourmaline is subhedral to anhedral and medium to large in size. It is seen as dark green under polarized light and in light green to pale orange in plane polarized light. Opaques are accessory minerals of this rock, making up 10 vol.% of rock in thin section. The secondary minerals of epidote, calcite, sericite, chlorite and iron oxides are generated due to the degradation of plagioclase and pyroxene (Fig 4a).

4.3. Trachyte

This rock is as gray and pink to pale gray in the field and in the hand specimen. Under a microscope, plagioclase phenocrysts appear as highly degraded, and pyroxene crystals are anhedral (Fig 4b) with a porphyritic texture. Plagioclase crystals are euhedral to subhedral and can be seen in small to medium sizes. They have polysynthetic twinning and often degraded along with the twins and exhibit a malachite facies. Some plagioclases are completely degraded to chlorite and calcite. Based on the extinction angle, the measured plagioclageses are oligoclase-andesine (An_{28-36}). They make up 40 to 45 vol.% of the rock in thin section. Pyroxenes are often decomposed and only remain in traces. Under the microscope and in polarized light, they appear in yellow to orange interference colors. There are often iron oxides or opaque and make up about 10 vol.% of the rock in thin section. The secondary minerals of these rocks are calcite, chlorite, clay minerals and iron oxides, which are obtained from the decomposition of plagioclase and pyroxene.

4.4. Dacite

This rock appears as light gray in the hand sample. The microscope view of the mineral indicates plagioclase crystals in a glassy and microcrystalline matrix. The texture of the stone is porphyritic. Plagioclase is euhedral, subhedral, and anhedral and makes up 30 to 35 vol.% of the rock matrix. Based on the extinction , the measured plagioclageses are oligoclase (An_{26-28}). these feldspars are oligoclase. The alteration process converts them to calcite, chlorite, , quartz, and iron oxides, making the minerals' surface cloudy. Quartz is found in small amounts and often as microcrystals in the rock matrix. The secondary minerals of these rocks are iron oxides, including hematite, magnetite, and limonite. Calcite, chlorite, sericite, iron oxides, and remnants of amphibole and biotite are visible in the rock. Iron oxides appear as inclusions inside the plagioclase crystals (Fig 4c).

4.5. Rhyodacite tuffs

These rocks appear in gray to dark gray and aphanitic in the hand sample. Under the microscope, they are highly decomposed and look like lithic tuff. The matrix is comprised of calcite, zeolite, and iron oxides. The texture of the rock is micro hialoporphyritic. Plagioclase of the major minerals of this rock, except for a few cases that have been decomposed and are difficult to identify. This mineral is of andesine type based on the intact samples' extinction angle measurements (An30-32). Quartz microcrystals are scattered in the rock matrix, and no other major minerals can be identified. The secondary minerals of these rocks are calcite, chlorite, iron oxides and clay minerals that form the rock matrix. The rock cavities are filled with zeolite. In addition, rock fragments are seen in the rock matrix, which is composed of plagioclase microlites.

4.6. Andesitic tuff

These rocks appear gray in the hand sample. Under the microscope, it contains plagioclase phenocrysts in a microcrystalline and microlithic matrix. They have porphyritic and microlithic porphyritic textures. Plagioclase crystals have polysynthetic twins decomposed into calcite, chlorite, sericite, and epidote along the twining margins. Based on the extinction angle, the measured plagioclageses (An_{28-36}) are andesine (Fig 4d). They are subhedral to anhedral and appear as microcrystals to medium crystals. These minerals constitute about 5 vol.% of rock. Iron oxides are the accessory minerals of the rock, making up about 3 vol.% of the rock. The secondary minerals of these rocks are chlorite, calcite, epidote, along with iron oxides of goethite, hematite, and magnetite type, generated due to the decomposition of plagioclase and mafic minerals. The rock matrix is strongly calcitized.

4.7. Trachy andesitic

This sample appears gray to a dark gray in hand sample. Under the microscope, it is highly decomposed. The rock matrix consists of calcite, zeolite, and iron oxides. The texture of the rock is porphyritic and microlithic. Plagioclase is one of the main minerals of this rock. Except for a few cases, all of them have been decomposed. According to the extinction angle , the measured plagioclageses are oligoclase-andesine (An_{38-44}). No other major minerals are identified in thin sections. The accessory minerals of the rock are iron oxides that are found in the rock matrix. Also, the secondary minerals of these rocks are calcite, chlorite, epidote, and iron oxides, which form the rock matrix (Fig 4e and 4.f).

5. Geochemistry of rocks in the study area

Chemical effects of different processes, including fractional crystallization, magma mixing, contamination, or a mixture of these processes, can be identified by geochemical studies on the distribution of different elements in the rock units of each region. The association between these elements is one of the most important aspects considered in geochemical studies. Using these relationships allows understanding the environments and processes effective in rock evolution (Table 1 and 2).

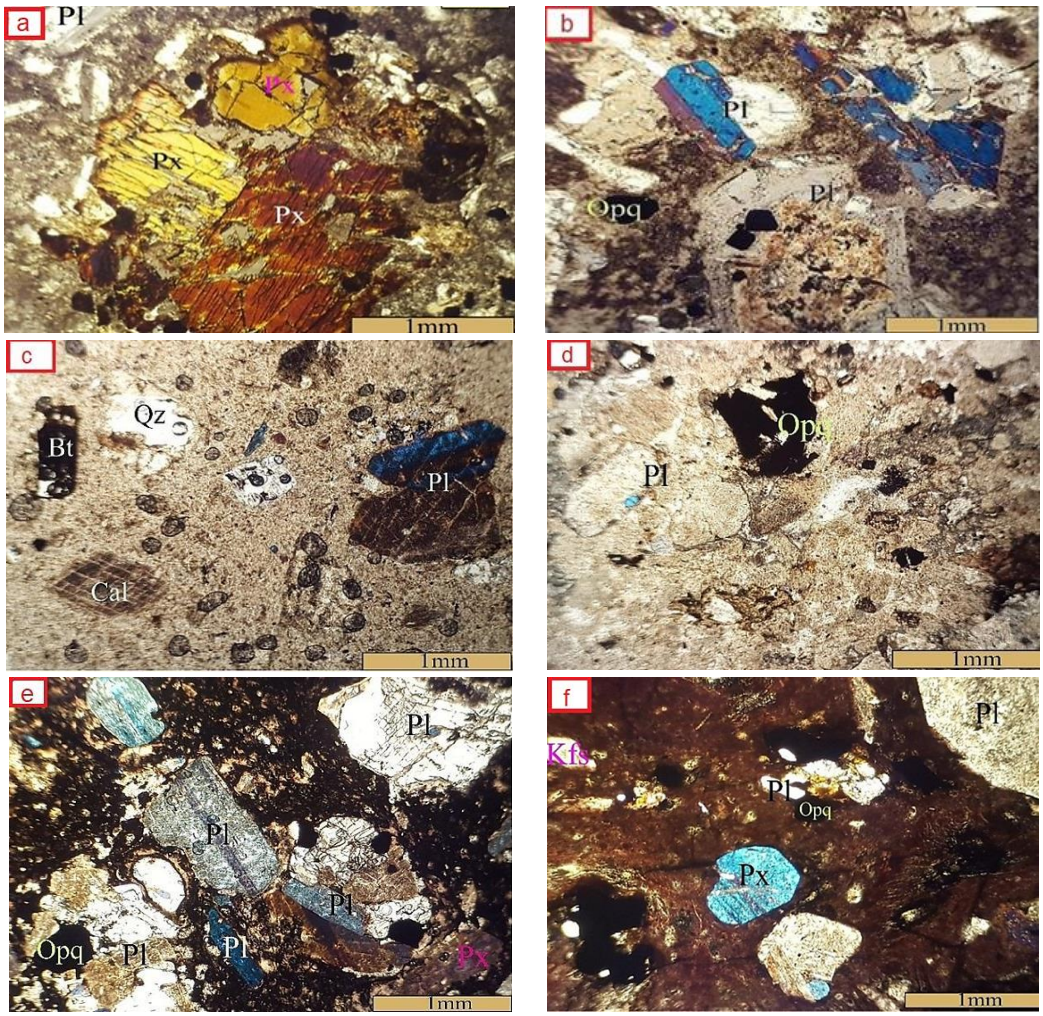

Fig 4 a- Plagioclase and pyroxene crystals in andesite b- Euhedral and subhedral plagioclase crystals and opaque minerals in trachyte. c- Plagioclase, biotite, calcite, and quartz crystals in dacite. d-Decomposed plagioclase and opaque minerals in andesitic tuff. e-Presence of plagioclase, pyroxene and opaque minerals in trachyandesite. f-Saussuritized plagioclase with mafic minerals in andesitic or andesitic tuff

The volcanic rocks of southeast of Abhar have high SiO_2 content (78.11.58 wt.%) and high K_2O + Na_2O content (11.8-0.38 wt.%). Normative minerals obtained from 20 rock samples include quartz (3.81-42.56), orthoclase (15.16-45.07), albite (8.14-40.74), anorthite (1.01-19.15), diopside (4.63-0.23), hypertension (0.15-4.14), magnetite (0.17-0.64), hematite (1.03-5.96), apatite (0.16-0.75) in all samples. Albite and orthoclase account for the largest percentage of these samples. Diopside and hypersthene are not seen in some specimens. A small number of these specimens have a low corundum concentration in their norm (in the norm of basalts, no corundum is seen at all). Also, geochemical classification diagrams (Le Bas et al. 1986), in the samples fall in the fields of trachy-andesite, trachyte, trachy dacite, andesite, rhyolite and dacite and (Fig 5a). According to the variation diagram of SiO_2 versus the total alkali Na_2O + K_2O (Kermantsky et al. 1980), they fall in the range of intermediate to acidic (i.e., andesite-andesite dacite, dacite, trachyte-alkaline trachea, trachyandesite, and rhyodacite-rhyolite) rocks (Fig 5b). Tholeiitic, calc-alkaline, high potassium calc-alkaline, and shoshonitic rocks were identified using K_2O versus SiO_2 diagrams (Le Bas et al. 1986). The rocks of the study area are in the range of high potassium calc-alkaline to shoshonitic (Fig 5c). Based on the Na_2O versus K_2O diagram (Le Maitre 2002), the volcanic samples southeast of Abhar show a shoshonite nature (Fig 5d). The genesis of shoshonite magmas has been attributed to the partial melting of the metasomatic lithosphere mantle (Conceição and Green 2004). The segregation of aqueous fluids and their reaction with the mantle leads to the formation of potassium magmas, which is also confirmed by experimental data (Wiley and Skin 1982; Jiang et al. 2002).

Table 1. (Continued). Whole rock geochemical compositions of the Eocene volcanic rocks from SE of Abhar area (major elements in wt.%, trace and rare earth elements in ppm).

Samples	M-01	M-02	M-03	M-04	M-06	M-07	M-10	M-12	M-14	M-15
Rock	Dacite			Andesite		Dacite		Rhyolite		
Major element (wt.%)										
SiO_2	65.28	65.53	64.36	58.85	54.38	63.89	64.94	74.27	75.29	78.11
TiO_2	0.45	0.45	0.44	0.57	0.56	0.44	0.65	0.33	0.29	0.24
Al_2O_3	15.34	15.28	14.90	16.32	15.66	14.74	13.91	12.74	11.70	11.08
TFe_2O_3	4.54	3.81	4.30	5.99	4.06	3.90	3.16	2.54	1.14	1.59
MnO	1.46	0.59	1.63	0.94	1.70	0.88	0.25	0.06	0.20	0.08
MgO	0.08	0.13	0.10	0.13	0.18	0.12	0.06	0.08		
CaO	3.38	3.62	4.14	5.47	8.57	4.13	4.27	0.20	2.00	1.70
Na_2O	3.63	3.27	3.30	3.80	3.69	3.14	4.55	0.95	2.67	3.98
K_2O	3.93	3.85	4.01	3.34	2.89	3.72	2.42	7.52	3.71	2.77
P_2O_5	0.17	0.14	0.18	0.16	0.16	0.14	0.19		0.09	0.08
BaO	0.07	0.06	0.07	0.06	0.05	0.06	0.06	<	<	<
LOI	1.67	3.27	2.57	4.30	8.04	4.84	5.40	1.23	2.85	0.28
Total	100.00	100.00	100.00	100.00	99.99	100.00	99.99	100.00	100.00	99.99
$Mg^{\#}$	44	27	48	27	50	35	16	5	30	11
Li	36.00	27.00	33.00	38.00	31.00	38.00	51.00	18.00	29.00	21.00
Be	1.90	1.80	1.80	1.80	1.50	1.80	1.20	2.20	1.10	1.70
Sc	9.60	9.50	9.00	11.60	11.60	8.80	10.70	5.70	3.60	2.80
V	85.00	83.00	80.00	116.00	110.00	76.00	99.00	9.00	26.00	32.00
Cr	25.00	26.00	26.00	34.00	27.00	28.00	36.00	26.00	38.00	26.00
Co	9.80	6.90	8.60	14.70	6.10	7.00	6.30	1.00	1.00	1.00
Ni	7.00	5.00	6.00	6.00	4.00	6.00	8.00	4.00	6.00	6.00
Cu	31.00	29.00	27.00	21.00	42.00	29.00	59.00	18.00	13.00	12.00
Zn	50.00	53.00	50.00	88.00	36.00	43.00	12.00	26.00	27.00	8.00
Rb	80.00	74.00	121.00	69.00	57.00	97.00	44.00	161.00	101.00	85.00
Sr	315.00	341.00	299.00	372.00	380.00	257.00	96.80	41.50	399.00	154.00
Y	21.30	21.70	21.60	22.40	22.00	20.00	22.70	40.90	11.90	10.80
Zr	75.00	79.00	76.00	78.00	72.00	80.00	203.00	523.00	69.00	55.00
Nb	17.60	10.50	16.90	14.60	11.80	12.60	14.10	27.80	10.80	13.00
Cs	2.60	1.90	2.80	2.00	1.60	2.40	3.60	2.70	1.00	0.50
Ba	924.00	880.00	880.00	770.00	640.00	848.00	856.00	578.00	544.00	466.00
La	27.00	28.00	26.00	25.00	25.00	26.00	26.00	65.00	44.00	25.00
Ce	51.00	51.00	50.00	47.00	47.00	49.00	59.00	149.00	71.00	49.00
Pr	5.59	4.40	5.70	5.55	5.13	5.46	6.21	14.45	6.92	4.90
Nd	20.20	15.80	20.60	20.30	19.10	19.50	23.10	53.80	22.80	16.20
Sm	3.90	2.88	4.09	3.89	3.45	3.82	4.68	10.44	3.23	2.30
Eu	1.54	1.17	1.56	1.58	1.39	1.53	1.65	1.53	1.05	0.76
Gd	3.39	2.65	3.28	3.32	3.06	3.15	3.55	6.94	3.11	2.47
Tb	0.57	0.46	0.59	0.60	0.54	0.55	0.62	1.14	0.44	0.37
Dy	3.59	2.59	3.65	3.78	3.30	3.32	3.89	6.93	2.09	1.75
Er	2.05	1.49	2.15	2.13	1.88	1.94	2.23	4.02	1.13	0.96
Tm	0.33	0.23	0.36	0.35	0.29	0.32	0.36	0.63	0.19	0.15
Yb	2.10	1.90	2.00	2.60	1.90	1.80	1.70	2.10	0.70	0.80
Ta	1.01	1.14	2.00	0.99	0.89	0.90	0.96	1.49	0.87	1.13
W	1.10	1.20	2.00	1.20	1.10	1.10	1.50	1.70	1.20	<1
Pb	1.00	1.00	3.00	1.00	1.00	1.00	1.00	1.00	42.00	1.00
Th	10.90	7.53	10.40	8.30	6.48	9.37	8.87	17.96	15.13	14.57
U	2.70	2.30	2.70	2.20	2.60	2.70	2.90	3.70	3.17	3.40
Hf	2.38	1.79	2.63	2.39	1.96	2.49	5.17	12.42	2.20	1.79

Table 2. (Continued). Whole rock geochemical compositions of the Eocene volcanic rocks from SE of Abhar area (major elements in wt.%, trace and rare earth elements in ppm)

Samples	**M-16**	**M-17**	**M-18**	**M-155**	**M-161**	**M-168**	**M-172**	**M-183**	**M-195**	**M-198**
Rock	Rhyolite			Trachyte – Trachy dacite					Dacite	Trachyte
Major element										
SiO_2	67.24	71.44	75.61	59.10	58.84	62.38	59.02	62.86	62.44	63.32
TiO_2	0.29	0.12	0.13	0.77	0.78	0.73	0.77	0.72	0.68	0.71
Al_2O_3	12.48	10.66	11.26	17.19	17.32	15.71	17.14	15.92	15.44	15.85
TFe_2O_3	2.02	1.18	1.69	5.41	5.32	4.44	5.41	4.41	4.32	4.39
MnO	0.11	0.59	0.12	1.40	1.58	1.22	1.49	1.40	1.58	1.41
MgO	0.07	0.09	0.05	0.11	0.12	0.10	0.10	0.07	0.07	0.07
CaO	4.74	4.32	1.54	4.09	3.98	1.62	3.83	1.63	2.65	1.45
Na_2O	3.96	2.19	2.44	4.14	3.53	3.94	3.69	3.83	2.86	3.65
K_2O	4.22	4.30	4.52	6.00	6.13	7.14	6.28	7.12	5.11	6.83
P_2O_5	0.09	0.07		0.34	0.36	0.27	0.32	0.24	0.23	0.25
BaO	0.06	<	<	0.07	0.07	0.08	0.09	0.08	0.07	0.08
Mg#	**12**	**54**	**14**	**38**	**42**	**40**	**40**	**43**	**47**	**44**
LOI	4.66	4.95	2.64	1.32	1.85	2.26	1.80	1.71	4.55	1.88
Total	99.94	99.98	100.00	99.94	99.94	100.01	99.94	99.99	100.00	100.01
Li	18.00	32.00	20.00	14.00	26.00	27.00	21.00	24.00	48.00	29.00
Be	1.10	2.40	2.30	3.50	3.50	4.00	3.40	4.10	3.10	4.20
Sc	3.30	2.40	2.20	11.30	10.80	9.20	10.40	9.00	8.60	9.60
V	33.00	27.00	26.00	99.00	105.00	66.00	100.00	64.00	79.00	64.00
Cr	16.00	19.00	24.00	30.00	24.00	26.00	28.00	31.00	27.00	29.00
Co	1.00	1.90	1.00	9.80	10.50	5.60	8.30	5.70	5.30	5.00
Ni	3.00	9.00	10.00	6.00	7.00	7.00	10.00	7.00	4.00	6.00
Cu	27.00	15.00	11.00	56.00	18.00	25.00	25.00	19.00	25.00	20.00
Zn	33.00	66.00	21.00	55.00	28.00	69.00	61.00	35.00	214.00	32.00
Rb	93.00	104.00	87.00	139.00	152.00	192.00	131.00	141.00	108.00	165.00
Sr	123.00	152.00	82.10	530.00	516.00	279.00	548.00	380.00	127.00	398.00
Y	11.60	10.10	7.00	30.50	29.10	31.60	28.70	30.80	30.00	32.50
Zr	48.00	74.00	81.00	248.00	259.00	325.00	252.00	320.00	317.00	329.00
Nb	9.30	11.40	13.10	19.20	18.80	23.00	20.10	22.80	21.20	22.00
Cs	0.70	0.50	0.50	1.10	0.70	0.90	2.40	0.50	2.00	0.80
Ba	654.00	442.00	417.00	969.00	900.00	1041.00	1127.00	990.00	955.00	1021.00
La	20.00	10.00	24.00	36.00	36.00	35.00	33.00	37.00	37.00	40.00
Ce	35.00	25.00	54.00	81.00	80.00	84.00	77.00	88.00	84.00	93.00
Pr	3.96	2.90	5.09	8.35	8.20	8.48	8.37	8.96	8.45	9.28
Nd	13.70	10.70	16.10	31.80	30.60	32.70	31.40	32.60	31.30	33.60
Sm	2.16	1.66	2.02	6.28	6.19	6.72	6.37	6.67	6.11	6.81
Eu	0.86	0.66	0.56	1.97	1.89	2.04	2.12	1.83	1.76	1.93
Gd	2.20	1.96	2.40	4.42	4.48	4.66	4.57	4.74	4.33	4.75
Tb	0.36	0.33	0.32	0.77	0.76	0.81	0.78	0.83	0.74	0.83
Dy	1.79	1.55	1.35	4.76	4.85	5.27	4.99	5.40	4.72	5.30
Er	0.96	0.79	0.66	2.66	2.76	3.10	2.73	3.22	2.74	3.07
Tm	0.16	0.14	0.11	0.40	0.44	0.51	0.44	0.51	0.44	0.49
Yb	0.80	0.70	0.70	2.60	2.50	2.40	2.50	2.40	2.30	2.50
Lu	0.21	0.21	0.18	0.43	0.48	0.57	0.50	0.59	0.49	0.58
Ta	0.71	0.81	0.93	1.10	1.19	1.51	1.32	1.41	1.20	1.13
W	1.10	1.80	1.50	2.20	2.60	2.50	2.70	2.90	3.60	3.00
Pb	1.00	1.00	1.00	5.00	12.00	5.00	6.00	25.00	34.00	26.00
Th	11.53	21.20	25.13	18.38	15.78	18.99	15.71	19.22	18.51	19.28
U	2.70	2.60	2.90	4.30	4.30	5.30	4.80	5.40	5.30	5.30
Hf	1.43	2.18	2.55	5.49	6.28	7.81	6.13	8.14	7.03	7.68

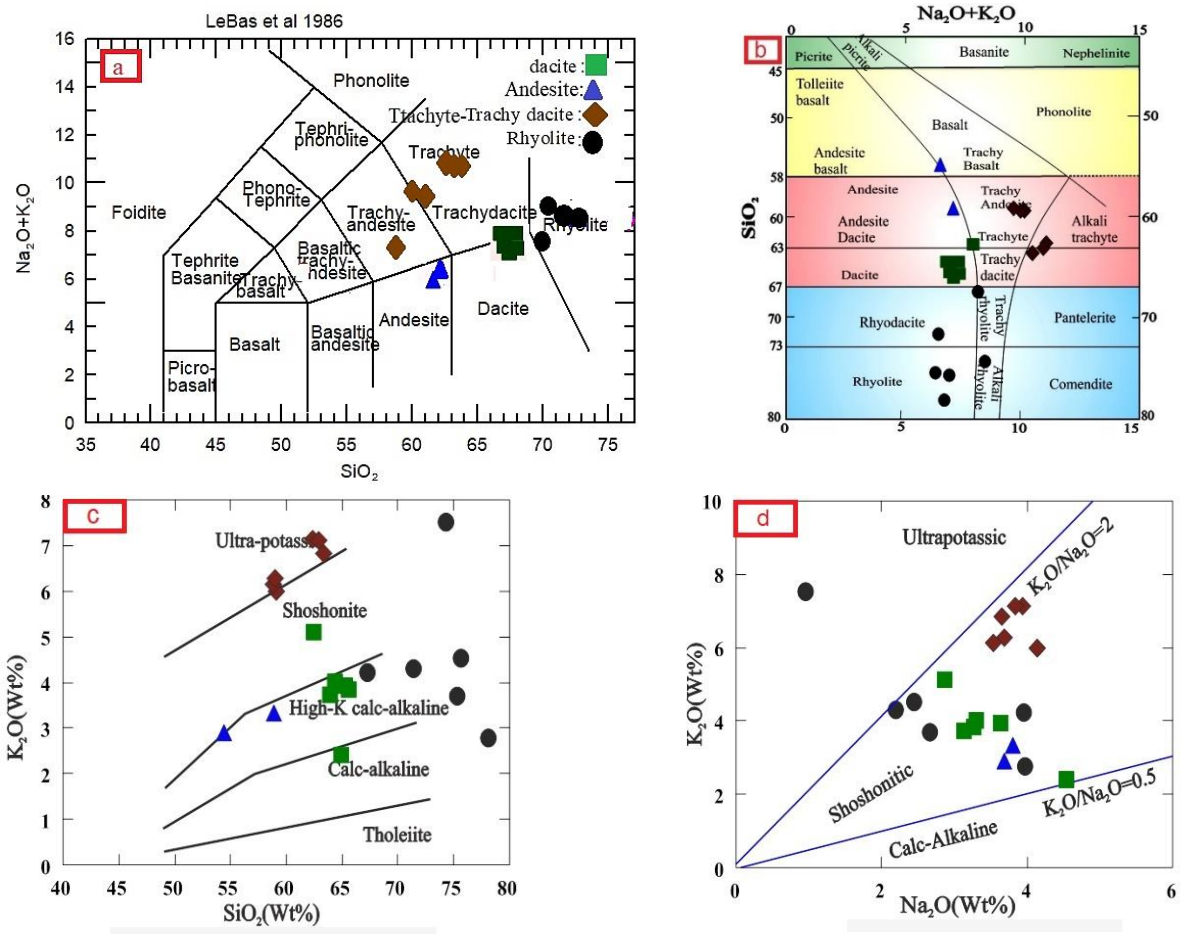

Fig 5. Geochemical classification diagrams: a- Na_2O+K_2O vs SiO_2 (Le Bas et al. 1986). b- Chemical classification diagram of volcanic rocks of southeast of Abhar based on the changes of $Na_2O + K_2O$ versus SiO_2 (Kermantsky et al. 1980). c- K_2O versus SiO_2 diagram (Le Bas 1986); the volcanic rocks of the study area are in the range of high potassium calc-alkaline to shoshonitic; d- Na_2O versus K_2O diagram (Le Maitre 2002); volcanic specimens of southeast of Abhar are located in the range of Shoshonite rocks.

Subduction-related magmas are characterized by enrichment of large ion lithophile elements (LILEs), light rare earth elements (LREEs) and depletion in high field strength elements (HFSEs) (Harangi et al. 2007). These geochemical signatures of magmatic rocks are commonly
explained by the addition of hydrous fluids from subducting oceanic lithosphere combined with the flux of melts from subducted sediments to the mantle wedge, lowering the mantle solidus and leading to magma generation (Aydınçakır 2016).
As shown in the spider diagram normalized to the primitive mantle (Sun and McDonough 1989) (Fig 6.a), the volcanic rocks of southeast of Abhar show enrichment in LILEs (K, Rb, Pb and Cs) relative to HFSEs (Ti (Yb, P and Nb), which is the characteristics of arc magmas (Pearce and Peate 1995; Perfit et al. 1980). The studied samples in this diagram have clear positive anomalies in U, K and Pb and certain negative anomalies in Ba, Sr, Nb and Yb. These observations suggest that minerals such as plagioclase, biotite and alkali feldspar are more differentiated in these samples. In addition, the studied volcanic rocks are relatively depleted at Ti and P indicating a source with high contents of titanium-bearing minerals (e.g., rutile, ilmenite, and titanomagnetite) and apatite. In general, LILE enrichment is caused by the addition of water-soluble elements by fluids produced by melting a dehydrated subduction plate into a mantle wedge (Tatsumi et al. 1986). Meanwhile, due to the immobility of HFSE elements in fluids, HFSE depletion reflects the previous depletion of these elements in the mantle wedge (Elliott 2003). Therefore, the released fluids have higher LILE and LREE contents than HFSE. In addition to subduction magmatism, Ti and Nb anomalies are also attributed to two other factors: A) The characteristic feature of continental crustal rocks and participation in magmatic processes (Leuthold et al. 2013; Rollinson 1993) and B) it is a sign of depletion of these elements in the origin of the stability of the phases containing these elements during melting or segregation process (Vivo et al. 2003).

The chondrite-normalized volcanic rocks of southeast of Abhar (Nakamura 1974) (Fig 4b) show that these rocks have REE differentiated patterns with a positive anomaly in Eu (Eu/Eu*=1.04-1.36) (Fig 5b). The positive Eu anomaly can be explained that this element has accumulated in the remaining melt. Therefore, Eu has a capacity of +3 and has not entered the plagioclase mineral. In these rocks, the (La/Yb) N and (Ce/Yb) N ratios in the studied samples vary from 6.43 to 42.03 and 0.43 to 25.80. These ratios, in other words, the slope of the patterns, are like the alkaline continental basalts (Beccaluva et al. 2002; Cook et al. 2005).

The depletion of HREEs relative to MREEs and LREEs and the increase in the LREE/HREE ratio can be attributed to the presence of garnet in the mantle source (Saccani 2015), the high depth of melting point, and the low partial melting rate in the source region (Rollinson 1993).

Garnet incorporates heavy elements (HREE) into its structure and prevents them from entering the magma. Enrichment of HSFEs and LREEs in alkaline basalts also indicates that they are directly derived from mantles such as OIB origin or melts with low degrees of melting (Xu et al. 2015). The remarkable negative anomaly of Nb, Ti, Eu, Sr in acidic and intermediate lavas including andesite, dacite and rhyolite is comparable with that in calc-alkaline subduction-related lavas (Kuscu and Geneli 2010; Litvak et al. 2015; Yang et al. 2015; Qian et al. 2016 and 2017; Ersoy et al. 2017; Sarem et al. 2021).

The existence of a linear and coordinated pattern between the trace elements seen in the Nakamura diagram (Fig 4b) may confirm the results obtained in the previous sections on the same origin of these rocks. They also suggest fractional crystallization as the main mechanism in the formation and evolution of these rocks.

Abhar volcanic rocks are a part of the Alborz-Azerbaijan zone. The tectonic basin of these rocks was evaluated using some diagrams designed based on the immobile REEs' abundance versus alteration and weathering processes (Pearce et al. 1984). When plotted on 100 Th/Zr versus 100Nb/Zr diagram (Pearce 1983), all of the rock samples fall in subduction- related volcanic arc field (Fig 5a). The samples are plotted within the subduction setting and the active continental margin fields on the basis of Ta/Yb versus Th/Yb diagram (Pearce 1983) (Fig 6b).

Based on the Rb/30-Hf –Ta × 3 and Rb/10-Hf -Ta × 3 diagrams (Harris et al. 1986) in Figs 6.c and 6.d, most specimens are located in the volcanic arc and post-collisional field and show the post-collision tectonic setting. In La/Yb versus Nb/La diagram (Hollocher et al. 2012) most specimens are located in the volcanic arc (Fig 6.e).

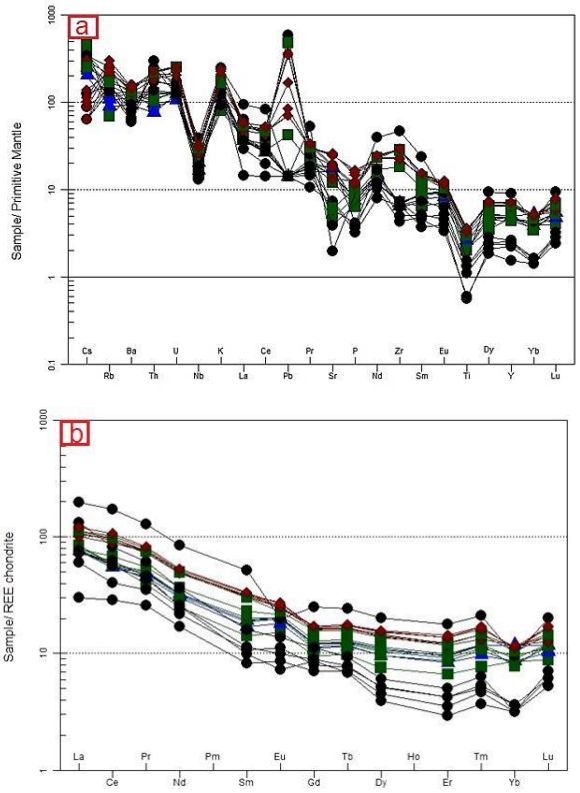

Fig 5. a- Diagram of trace element changes in the diagram normalized to primitive mantle composition (Sun and McDonough 1989) and b- Diagram of trace element changes relative to the chondrite-normalized diagram (Nakamura 1974).

Because the Ce/Pb and Nb/U ratios are very sensitive to crustal contamination (Furman 2007), they are commonly used to detect the occurrence of this type of contamination. Also, due to the lower Nb/U and Ce/Pb in the continental crust than in mantle-derived magmas, the Nb/U ratio in the studied samples is 47% lower than this ratio in mantle-derived magmas (Hofmann et al. 1986). This ratio in volcanic rocks of southeast of Abhar is 3.41-7.51. The low value of this ratio in the studied samples reflects crustal contamination's effect on these rocks (Fig 7.a). The relatively high values of some LILE elements and high Ba/Nb ratios indicate the effect of crustal components in the formation of these rocks due to magmatic impregnation during the magma upwelling from within the crustal rocks. The Nb/La versus Nb diagram (Xia et al. 2012; Fig 6.b) has also been used to determine crustal contamination. An Nb/La > 0.9 indicates weak crustal contamination or no contamination in the magma (Xia et al. 2012). Also, an Nb/La < 0.9 shows the geochemical properties of molten crustal contamination. As presented in Fig 7b, the Nb/La ratio in most volcanic samples in the area is less than 0.9, indicating crustal contamination in these rocks.

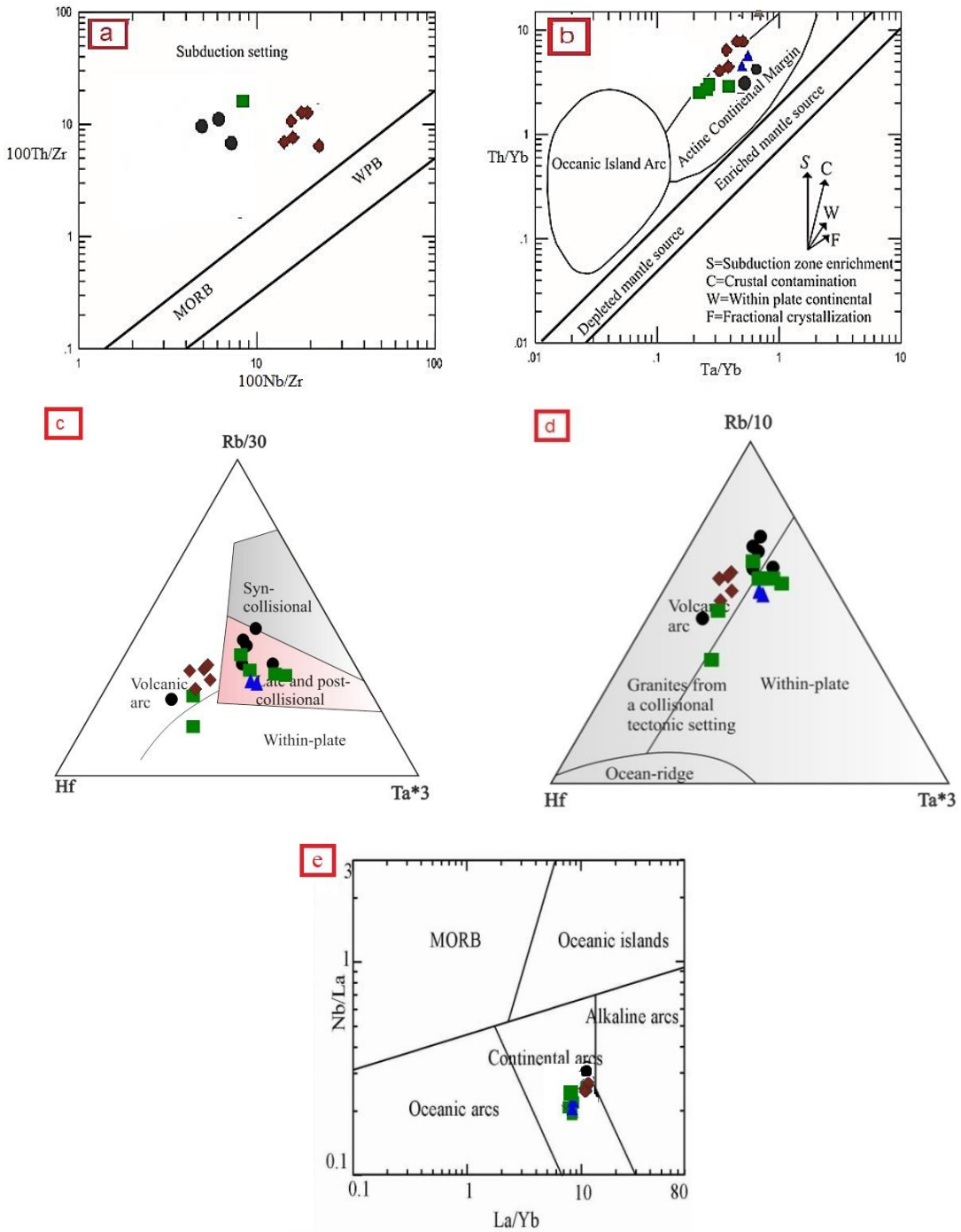

Fig 6. Differention diagrams of tectonic settings: a,b-100Th/Zr vs. 100Nb/Zr diagram and Ta/Yb vs. Th/Yb diagram, after Pearce (1983). c-Rb/30-Hf-Ta×3; d- Rb/10- Hf-Ta×3 (Harris et al. 1986). The samples are located in the VAG field and show a post-collisional tectonic setting. e-La/Yb versus Nb/La diagram (Hollocher et al. 2012)

The geochemical characteristics of the studied samples indicated that fractional crystallization (FC) is the primary cause of the diversity and differentiation of these rocks compared to crustal contamination. Low ratios of Nb/Ta = 10-20 versus SiO_2 (Fig 8.a) indicate a common genetic relationship between the studied volcanic samples and the evolution of these rocks through FC (Gounti´e Dedzo et al. 2019). Negative Nb-Ti and positive Pb anomalies (Fig 4), high La/Nb ratios (1.54-2.67), and low La/Ba (0.02-0.11) (Fig 7.b) in the studied samples show the typical features of a subduction lithospheric mantle (Saunders et al. 1992). Partial melting of subducted sediments and ocean-derived fluids can cause metasomatism and enrichment of the source zone of subduction-related magmas (Guo et al. 2007). Also, water-bearing melt has a much higher capacity to transport HFSEs than liquid phases, while LILEs can be transported more efficiently instead of

being melted by liquids (Herman et al. 2006; Chen et al. 2018). Therefore, the relative contribution of two metasomatic factors in the formation of the studied volcanic rocks can be sought using the ratio of trace elements with certain fluid mobility. As shown in Fig 7.c, the samples have varying degrees of Ba/La ratios (34/17-22/38), but Th/Yb ratios (2.14-35.90) are relatively uniform, suggesting the important role of fluids from slabs in their petrogenesis. To identify the role of slab-related fluids along with the enrichment trend, we used trace element variation diagrams of Sr/La vs. La/Yb and Th/Yb vs. Ba/La (Saunders et al. 1992) and Nb/Y vs. Rb/Y (Bhat et al. 2019) (Figs 8.c, 8.d, and 8.e). All diagrams provide evidence for plate metasomatism and represent a metasomatism-influenced mantle source for the studied samples.

The following diagrams indicate the role of fractional crystallization (FC) in the evolution of the region's lavas, the spread of felsic units on earth is more than that of basic units. According to Liu et al. 2014, the involvement of crustal components can occur as partial melting of sediments above the subducting plate or delamination. The high contents of SiO_2 (78.11-54.38 wt.%), Ce (25-93 ppm), and La (10-40 ppm) indicate the involvement of crustal materials in the region's magmatic evolution. If the Ce concentration in crustal materials is affected, either due to the partial melting of the sediments above the subducting plate or the partial melting of the crust (McDermott et al. 2005), Ce/Yb will change accordingly. In region rocks (Fig 7.c), Ce/Yb increased, especially in the samples investigated, suggesting the partial melting of crustal components and their effect on magmatic evolutions (Liu et al. 2014). Particularly, in acidic volcanic rocks, where crustal components have involved magma generation and evolution, it is not easy to distinguish the role of partial melting of crust from partial melting of sediments above the subducting plate (Temel et al. 1998; McDermott et al. 2005; Temizel and Arslan 2008; Liu et al. 2014).

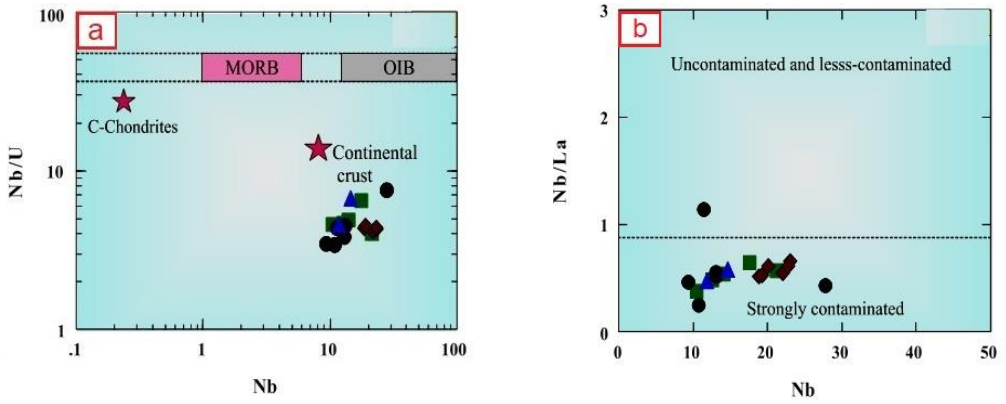

Fig 7. a-Nb/U vs. Nb diagram (Cornelius et al. 2011). b- Nb/La vs. Nb diagram (Xia et al. 2012) for the studied samples, showing the effect of crustal pollution on them.

According to Temel et al. 1998, the volcanism of the active continental margins has a Nb/Y ratio of less than 1.72, varying from 0.4 to 0.9 in the examined samples. If crustal components are involved in magma genesis, the range of Nb/U changes is low (5-10) (Conticelli et al. 2009). This ratio is 3.44-6.52 in the region's rocks, indicating the partial melting of crustal materials in the magma composition.

Th/Nb <0.3 and Th/La <0.25 can also be considered geochemical indicators of partial melting in the crust and the source rocks of the acid rocks of the region as Th/Nb in the rocks of the region is in the range of 0.55 to 1.92. Also, Th/La is 0.10-0.92, and the investigated rocks are consistent with the mentioned values. As mentioned before, although it is difficult to distinguish the magmas resulting from the partial melting of the sediments above the subducting plate from the magmas generated by the partial melting of the crust, some authors have tried to differentiate the magmas from the mentioned origins. Pelagic sediments above the subducting plate have Pb/Rb of 0.3-0.37, Pb/K_2O of 14-12, and Sm/Hf of 3. While the continental crust has lower ratios of Pb/Rb (0.2-0.15), Pb/K_2O and Sm/Hf are 0-8 and 1, respectively (Çoban et al. 2012). Regarding the ratios of Pb/K_2O (0.25-11.13), Pb/Rb (0.06-0.41), and Sm/Hf (1.25) in the examined volcanic rocks, it can be expected that crustal materials in intermediate basic magma contamination.

The Mg # values of the primary arc melts are usually greater than 70 (Schmidt and Jagotz 2017), compared to the studied rocks, which are less than 50, indicating that these volcanic rocks have formed in magma chamber composed of mantle-derived magma after fractional crystallization (Xu et al. 2019). This interpretation is supported by the low content of some compatible elements in volcanic rocks. For example, the Cr (16-38 ppm) and Ni (3-10 ppm) contents of the samples are significantly lower than the initial arc magma (i.e., Cr = 364 ppm and Ni = 168 ppm (Gudnason et al. 2012) Experimental studies on melting have shown that continental crustal melting is usually rich in sodium (Wiley and Rutter 1986).

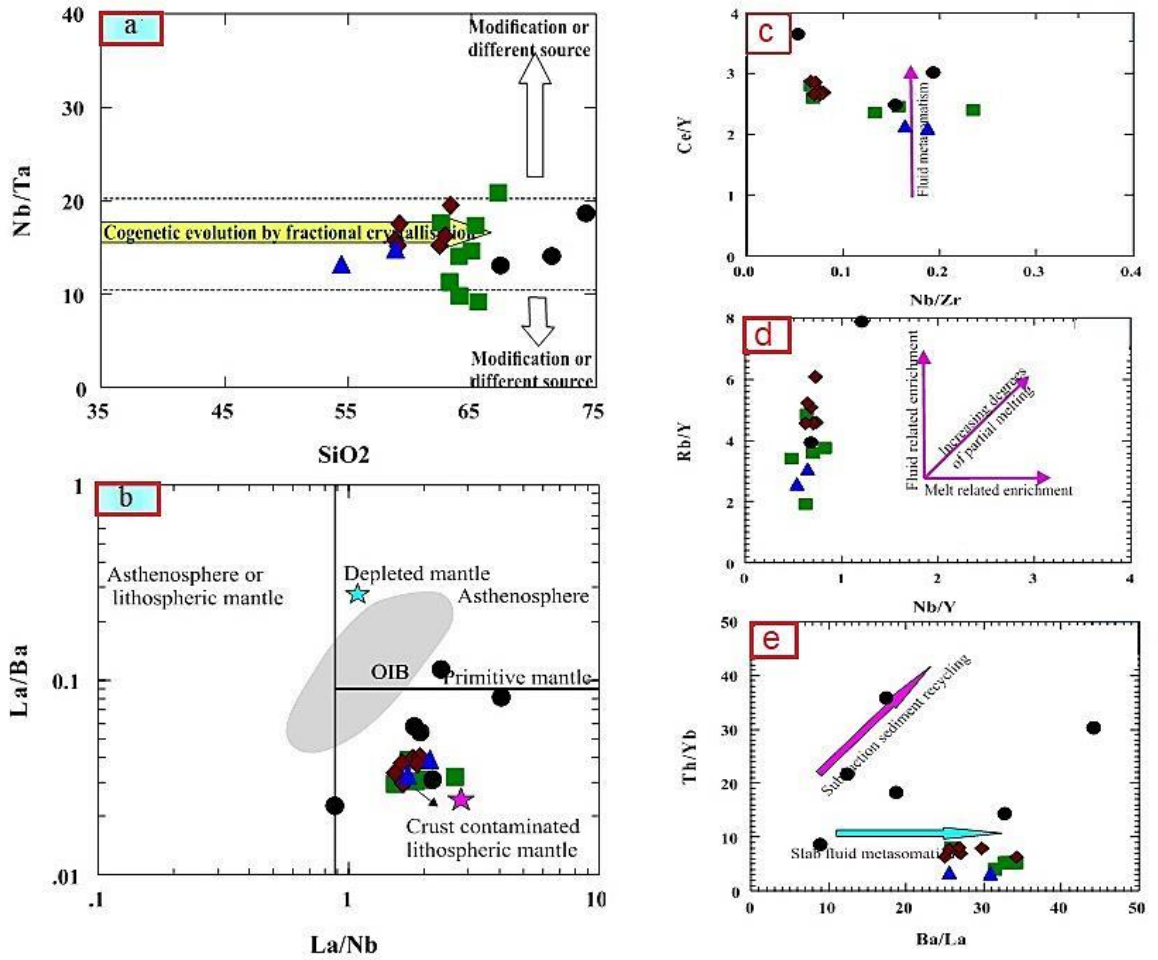

Fig 8. a-Nb/Ta diagram vs. SiO_2 (Marilyn Gontier Dezo et al. 2020); b- La/Ba diagram versus La/Nb (Saunders et al. 1992), showing evolution by fractional crystallization and a mantle continental lithosphere source for the studied samples; c- Ce/Y diagram vs. Nb/Zr; and d) Rb/Y diagram vs. Nb/Y (Bhat et al. 2019); e- Th/Yb vs. Ba/La (Saunders et al. 1992), showing the role of slab-related fluids.

6. Mantle source and enrichment processes

In the studied area, the spider diagrams normalized to chondrite and primary mantle show negative anomalies of Nb, Ti, Eu and Sr, which indicate the formation of rocks in subduction zone. According to Fig 9a, Abhra volcanic rocks originated from a subcontinental lithosphere source (Hooper and Hawkesworth 1993). A plot of Th/Yb vs. Nb/Yb shows the enriched mantle source with involvement of subduction zone components (Pearce 2008 After Ersoy et al. 2017) (Fig 9b). If the asthenospheric mantle sources are enriched by metasomatic processes related to subduction zone, the ratios of Nb/La and Nb/Ba (<0.47 and 0.02, respectively) are low (Ersoy et al. 2017), which are 0.6 and 0.05, respectively, in the studied rocks. The mineralogical composition of the mantle source is an important factor in the composition of the partial melt (whether it contains spinel or garnet) (Ersoy et al. 2017). Depletion of HREEs and values of Y and Yb less than 15 and 1.4 ppm, respectively, indicate the formation of melt from a source with melt slag in subduction zone (Drummond and Defant 1990). These values are between 16.3 and 25.7 (for Y) and 3.5 and 1.81 ppm (for Yb) in Abhar Volcanic rocks which approve the absence of residual garnets. The ratio of HFSE and REE elements are also used to identify the origin of rocks, for example, the diagram of Nb/Yb and Zr/Yb vs. Ta/Yb from (Pang et al. 2013), which shows an OIB-like mantle source for rocks in the Abhar region(Fig 9a,b). By using the Th/Yb versus La/Yb diagram (Ersoy et al. 2017), it is possible to understand the enrichment of the mantle source, the presence of lherzolite spinel or lherzolite garnet phase, as well as the absence or presence of residual garnets in the magmatic sources, that the rocks of the studied area are of a trend. They show the enrichment in the mantle source and the presence of lherzolite spinel phase (Fig 9c).

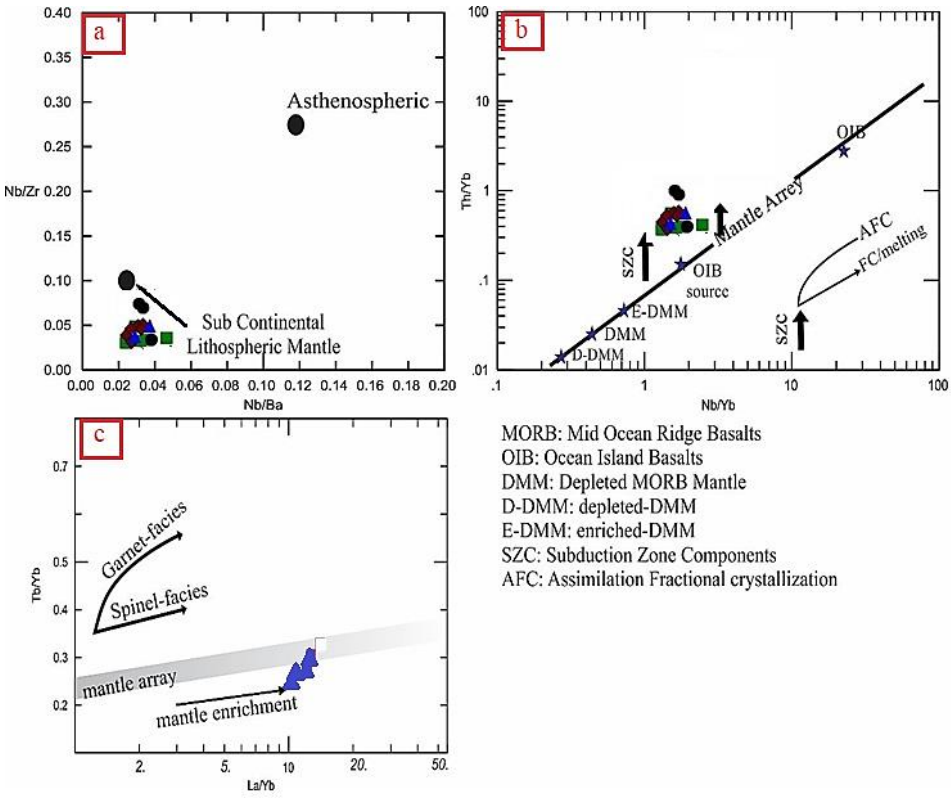

Fig 9. Whole-rock a- Nb/Ba versus Nb/Zr (ppm) (Hooper and Hawkesworth 1993). b- Th/Yb versus Nb/Yb (ppm) (Pearce 2008 and after Ersoy et al. 2017). c- Th/Yb diagram versus La/Yb (ppm) (Ersoy et al. 2017).

7. Techtono-magmatic setting

To detect the tectonic position of how generation of intermediate to acidic rocks are formed, various models have been presented so far. In this regard, it is thought that high magnesium andesites are formed in two ways: firstly partial melting of eclogitic and granulitic crust, Secondly partial melting of a young and hot subduction slab with adakitic nature (Qian et al. 2016 and 2017). Relative melting of an eclogitic-granulitic crust produces a melt with low rutile content, high Mg# and Al2O3>17% (Qian et al. 2017). The high Mg content (0.94-2.96%) and high Mg# (51.04 to 55.74), Al2O3 <17% in the rocks of the studied area show that the melting of part of the eclogitic-granulitic crust was not the effective factor for the formation of these rocks. The adakite melt, which has Sr, Al and Si > 400 ppm, Y < 18 ppm and Yb < 1.9 ppm, was obtained from the partial melting of a young subduction slab (Qian et al. 2017). But in volcanic rocks of Abhar region Sr is >400, Y>20 and Yb is >0.70 up to 2.60 ppm. To highlight the role of crustal pollution in the petrogenesis of rhyolitic rocks and other acidic rocks, isotopic ratios are used, which was previously done by Elahpour and his colleagues in 2016. Fluids released from the subducting oceanic slab that caused metasomatism are characterized by negative Nb anomalies and high Ba/Th and Ba/La ratios. Sediments on the subduction plane of high Th and high Th/Yb and Th/Nb ratios have also led to the phenomenon of metasomatism (Yang et al. 2015; Qian et al. 2017). The lack of Nb anomaly, high Th content (6.48-25.13), Th/Yb = 3.41-34.46 and Th/Nb = 0.65-1.42, a mantle source modified by the recycled sediments and melts released from the edge of the subducting oceanic crust are suggested for the formation of andesites and dacites in the region.

It seems that the rocks of the studied area (andesite, dacite) are composed of an OIB origin (such as mantle components) and partial melting of subcontinental lithospheric mantle. In relation to the petrogenesis of the rocks of the studied area, it can be inferred that a partially metasomatized melting source by the recycled sediment cycle of the subduction slab and a source close to the modified mantle were involved, such a theory was previously supported by Qian et al. (2016 and 2017) has been proven.

Petrology studies on the intrusive masses (Naderi and Aghazadeh 2013; Castro et al. 2013; Seyed Qaraini et al. 2019) belonging to the late Eocene-Oligocene have had almost the same results in the northern and southern slopes of Tarem mountains. Overall, the reviewed articles indicate that these masses are associated with the continental margin and active continental arc. However, some researchers attributed hybrid characteristics to these masses. This area is denoted by Area B in (Fig 10). Therefore, the Tarem mountains can be divided into two parallel sub-zones, south and north. From the tectonic point of view, the southern sub-zone is the location of the magmatic arc of the active

continental margin in the Eocene period, and the northern sub-zone is located in the back-arc area. The extensional movements of the back-arc basin have continued up to the incomplete rift. In addition, due to the compressive movements between Central Iran and the Turan Plate, the expansion of the rift has not continued much. In this regard, the effects of these compressive movements are due to the intrusion of granitoid masses of continental arcs or monzonites. Due to the large volume of eruptions that occurred in the late Eocene, a large amount of magma has erupted on the ground. Along with the ground's cooling, subsidence has gradually occurred in the Manjil-Gilvan-Dram area, and the Tertiary sediments have been deposited in this subsidence area.

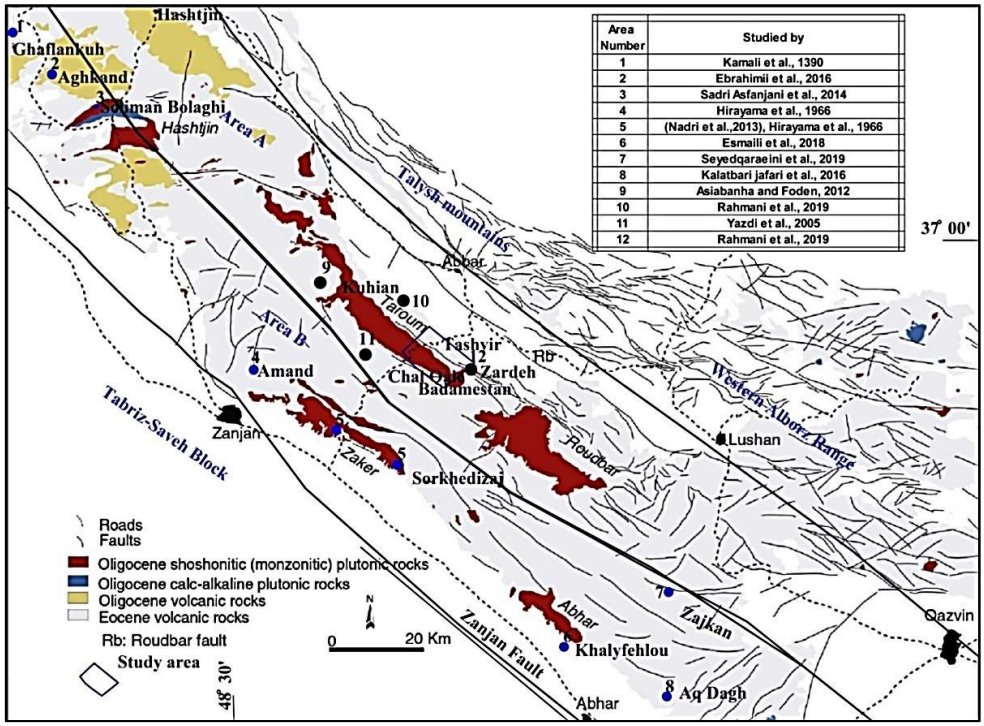

Fig 10. Location of petrological studies conducted in the Tarem Mountains; according to these studies, the Tarem area in the Eocene is divided into two zones: a) the northern incomplete rift basin and b) the magmatic arc.

Studying geochemical data of volcanic rocks in southeast Abhar indicates that fractional crystallization is a considerable process during magma evolution, and these rocks have formed due to (1) fractional crystallization of mafic mother magma and (2) the continental crust melting or AFC processes. This claim is supported by similar isotopic compositions and the pattern of planar changes in trace element concentrations or ratios between felsic and mafic rocks, emphasizing the common parent magma and the geochemical differentiation of mafic magma to felsic. As previously discussed, these rocks are metasomatized by subduction-dependent fluids. Therefore, it is suggested that these volcanic rocks originate from mantle-enriched material with the introduction of subduction-related materials. These rocks, which are formed by extensive fractional crystallization, are characterized by plagioclase, pyroxene, and biotite phenocrysts. In Fig 11, we present a schematic model for the formation of volcanic rocks (inspired by Paul et al. 2020). Mafic magma is primarily in the basin of the crust. Factors associated with the formation of magmatic chambers cause the fractional crystallization of the closed system (Natali et al. 2011). Fractional crystallization is a common phenomenon in a magmatic system by which mafic magma evolves upon cooling and forms a mixed chain of melts to form basalt-andesite-dacite-rhyolite (Rooney et al. 2010). Despite the ambiguities about volcanic rock formation, others have concluded that extensive fractional crystallization (often up to 95%) of primary mafic magma in a closed system (no crustal inlet) can produce a highly felsic magma (rhyolite) (Lightfoot et al. 1987; Cucciniello et al. 2019). This process is schematically shown in Fig 11. In general, one-tenth of the total magma erupts and forms volcanic rocks, while the remainder crystallizes to form plutonic rocks (Crisp 1984). (Annen and Sparks 2002) argued that early magma could provide some of the prematurely formed mafic rocks by providing the necessary heat where the surrounding crust is dehydrated (e.g., the lower mafic crust). As a result, low-grade partial melting (~ 10%), as well as pre-formed and underplated basalts (Fig 11), can typically produce magma with more silica (e.g., rhyolite).

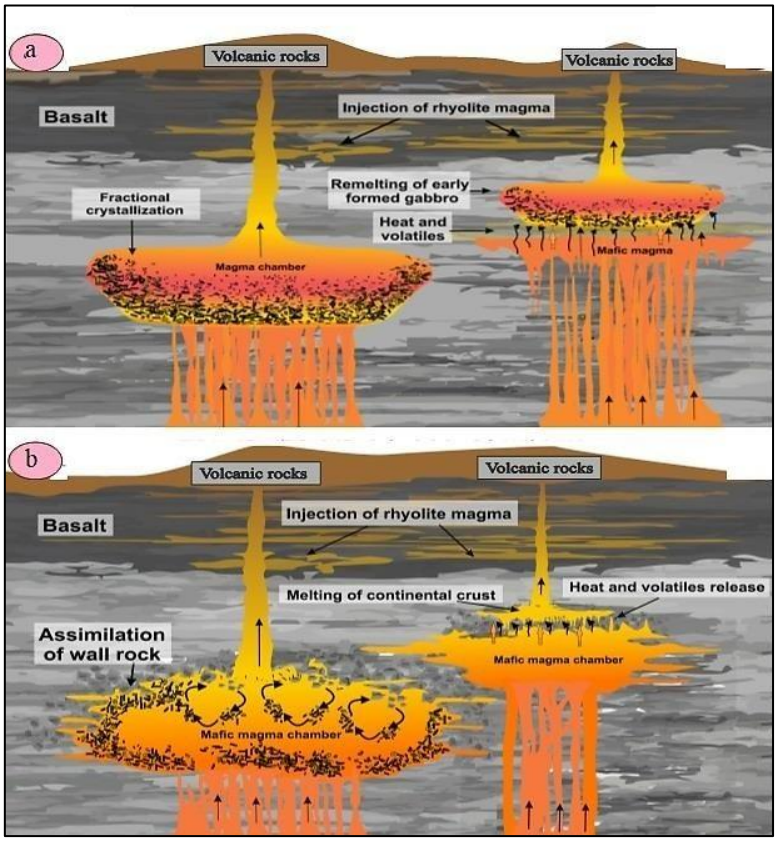

Fig 11. Schematic representation of petrogenetic processes responsible for the origin of rhyolite and other studied rocks. For simplicity, the method of producing the associated basalt is not shown. A- Extensive fractional crystallization of primary mafic magma in a closed system and deep in the crust forms rhyolite melts. Similarly, remelting of primary mafic magma (gabbro or basalt), due to the heat released from the mafic magma chamber, leads to the production of more acidic magmas (such as rhyolite); b- The assimilation of the surrounding continental crust synchronous with AFC or the melting of continental crustal material results in the formation of volcanic rocks with a more felsic composition.

8. Conclusion

According to field, mineralogy, petrographic, geochemical, and petrological studies of volcanic rocks in the southeast of Abhar, these rocks are composed of lava and pyroclastic rocks of the Karaj Formation. Also, the classification of these rocks based on their norm minerals calculation indicates that most of them are located in the field of quartz latite, rhyodacite, and rhyolite. On the other hand, based on chemical classification diagrams, these rocks plot in the trachyandesite, trachyte-trachy dacite, dacite, and rhyolite domain. Geochemical studies indicate that the samples are located in the calc-alkaline-alkaline and high potassium-shoshonitic domain. Therefore, these data confirm a metasomatic lithosphere mantle origin and the important role of fractional crystallization in the evolution of these rocks. Overall, the studied samples have formed in a volcanic arc basin related to the subduction of the oceanic crust. Calc-alkaline lavas of this area indicate a subduction zone and active continental margin setting which are relatively enriched in LILE and LREE elements compared to HREE and HFSE elements and they are depleted in Nb, Ti, Sr, P and Eu.

References

Alavi M (1994) Tectonics of the Zagros orogenic belt of Iran: New data and interpretations. *Journal of Tectonophysics* 299: 211 – 238.

Annells RN, Arthurton RS, Bazely RA, Davies RG (1975) Explanatory text of the Qazvin and Rasht quadrangle map1:250000, GSI. Rep., nos. E3, E4: 94.

Annen C, Sparks RSJ (2002) Effects of repetitive emplacement of basaltic intrusions on thermal evolution and melt generation in the crust. *Earth Planet* 203: 937–955.

Asiabanha A, Foden J (2012) Post-collisional transition from an extensional volcano-sedimentary basin to a continental arc in the Alborz Ranges, N-Iran, *Journal of Lithos* 148: 98-111.

Aydınçakır E (2016) Subduction-related Late Cretaceous high-K volcanism in the Central Pontides orogenic belt: Constraints on geodynamic implications. *Journal of Geodinamica Acta* 28(4): 379–411.

Beccaluva L, Coltorti M, Di Girolamo P, Melluso L, Milani L, Morra V, Siena F (2002). Petrogenesis and evolution of Mt. Vulture alkaline volcanism (Southern Italy). *Mineralogy and Petrology* 74(2): 277-297.

Berberian M, King GCP (1981) Towards a paleogeography and tectonic evolution of Iran. *Canadian Journal of Earth sciences* 18(2): 210-265.

Bhat IM, Ahmad T, Rao DS (2019) The tectonic evolution of the Dras arc complex along the Indus Suture Zone, western Himalaya: Implications for the Neo-Tethys Ocean geodynamics, *Journal of Geodynamics* 124: 52–66.

Castro A, Aghazadeh M, Badrzadeh Z, Chichorro M (2013) Late Eocene–Oligocene post-collisional monzonitic intrusions from the Alborz magmatic belt, NW Iran. An example of monzonite magma generation from a metasomatized mantle source. *Lithos* 109–127.

Chen L, Zheng YF, Zhao ZF (2018) A common crustal component in the sources of bimodal magmatism: geochemical evidence from Mesozoic volcanics in the Middle-Lower Yangtze Valley, South China, *Journal of Geological Society of America Bulletin* 130: 1959–1980.

Çoban H, Karacık Z, Ece ÖI (2012) Source contamination and tectonomagmatic signals of overlapping Early to Middle Miocene orogenic magmas associated with shallow continental subduction and asthenospheric mantle flows in Western Anatolia: A record from Simav (Kütahya) region. *Lithos* 140, 119-141.

Conceição RV, Green DH (2004) Derivation of potassic (shoshonitic) magmas by decompression melting of phlogopite+pargasite lherzolite, *Journal of Geology* 72: 209-229.

Conticelli S, Guarnieri LI, Farinelli A, Mattei M, Avanzinelli R, Bianchini G, Boari E, Tommasini S, Tiepolo M, Prelevic D, Venturelli G (2009) Trace elements and Sr-Nd-Pb isotopes of K-rich, shoshonitic, and calc-alkaline magmatism of the Western Mediterranean Region: genesis of ultrapotassic to calc-alkaline magmatic associations in a post-collisional geodynamic setting, *Lithos* 107: 68-92.

Cook C, Briggs RM, Smith IEM, Maas R (2005) Petrology and geochemistry of Intraplate Basalts in the South Auckland Volcanic Field, New Zealand: Evidence for Two Coeval Magma Suites from Distinct Sources. *Journal of Petrology* 46(3): 473- 503.

Cornelius T, Ntaflos Th, Akinin V (2011) Polybaric petrogenesis of Neogene alkaline magmas in an extensional tectonic environmeniv: Viliga Volcanic Field, northeast Russia. *Lithos* 122, 13 –24.

Crisp JA (1984) Rates of magma emplacement and volcanic output, *Journal of* Volcanology 20: 177–211.

Cucciniello C, Choudhary AK, Pande K, Sheth H (2019) Mineralogy, geochemistry and 40 Ar–39Ar geochronology of the Barda and Alech complexes, Saurashtra, northwestern Deccan Traps: early silicic magmas derived by flood basalt fractionation, *Geological Magazine:* 1– 23.

Dabiri R, Akbari-Mogaddam M, Ghaffari M. (2018) Geochemical evolution and petrogenesis of the eocene Kashmar granitoid rocks, NE Iran: implications for fractional crystallization and crustal contamination processes. *Iranian Journal of Earth Sciences* 10(1): 68-77.

De Vivo B, Lima A, Albanese S, Cicchella D (2003) AtlanteGeochimico-Ambientale della Regione Campania. De Frede Editore, Napoli. 214 pp.

Dedzo MG, Hamadjoda DD, Fozing E, Tchamabé BC, Mendoza-Rosas AT, Asaah A, Tefogoum GZ, Kamgang P, Ohba T (2020) Petrology and geochemistry of ignimbrites and associated enclaves from Mount Bambouto, West-Cameroon, Cameroon Volcanic Line. *Geochemistry journal* 80(4):1-46.

Didon J, Gemain Y M (1976) Le Sabalan, Volcan Plio-quaternair de l'Azerbaidjan oriental (Iran); etude geologique et petrographique de l'edifice et de son environnement regional. These de 3eme Cycle, Univ. *Grenoble* 304p.

Drummond MS, Defant MJ (1990) A model for trondhjemite, tonalite, dacite genesis and crustal growth via slab melting: Archean to modern comparisons. *Journal of Geophysical Research: Solid Earth* 95(B13): 21503-21521.

Ebrahimi M, Esmaeili R, Aouizerat A (2017) New geodynamical model for regional Tertiary extension during the Zagros orogeny: A transtensional arc? *Iranian Journal of Earth Sciences* 9(2): 115-120.

Ebrahimi M, Kohestani H, Mokhtari MAA, Faizi M (2015) Lithology and geochemistry of acidic volcanic rocks and perlites of Aghkand, north of Zanjan, *cientific Quarterly of Earth Sciences* 101:110-99.

Elahpour E, Vosoughi Abedini M, Pourmoafi SM (2016) Determination of parental melt nature and evolutions of volcanic rocks in Sarchah geological map area (southern Khorasan) based on isotopic data. *Iranian Journal of Geology* 10 (38): 103-113.

Elliott T (2003) Tracers of the slab. in Eiler, J., eds., Inside the subduction factory: Washington. American Geophysical Union, *Journal of Geophysical Monograph* 138: 23-45.

Emami MH, Ashja Ardalan A (2005) Petrology of Tarom Olya Plutonism (Kuhyan region) *Journal of Basic Sciences (Islamic Azad University)* 57:250-270.

Ersoy EY, Palmer MR, Genç ŞC, Prelević D, Akal C, Uysal İ (2017) Chemo-probe into the mantle origin of the NW Anatolia Eocene to Miocene volcanic rocks: Implications for the role of, crustal accretion, subduction, slab roll-back and slab break-off processes in genesis of post-collisional magmatism. *Lithos* 288: 55-71.

Esmaili M, Lotfi M, Nazafti N (2018) Mineralogy and genesis of Khalifalu copper deposit based on geochemical data of the host rock and S and O isotopic characteristics. *Earth Sciences Quarterly* 110: 33-46.

Furman T (2007) Geochemistry of East African Rift basalts: an overview, *Journal of African Earth Sciences* 48(2):147-160.

Gounti´e Dedzo M, Asaah ANE, Martial Fozing E, Chako-Tchamab´e B, Tefogoum Zangmo G, Dagwai N, Tchokona Seuwui D, Kamgang P, Aka FT, Ohba T (2019) Petrology and geochemistry of lavas from Gawar, Minawao and Zamay volcanoes of the northern segment of the Cameroon volcanic line (Central Africa):): Constraints on mantle source and geochemical evolution, *Journal of African Earth Sciences*153: 31–41.

Gudnason J, Holm PM, Søager N, Llambías EJ (2012) Geochronology of the late Pliocene to recent volcanic activity in the Payenia back-arc volcanic province, Mendoza Argentina. J. S. Am. *Journal of Earth Sciences* 37:191–201.

Guo Z, Wilson M, Liu Jiaqi (2007) Post-collisional adakites in south Tibet Products of partial: melting of subduction-modified lower crust. *Lithos* 96: 205-224.

Haghnazar Sh, Malakootian S (2013) Origin and tectonic environment of the volcanic rocks of Damash Gilan (northern Iran), *Iranian Geological Quarterly* 27:89-110.

Haghnazar Sh, Shafeii Z (2014) The role of MORB-mantle source and continental crust in genesis of Tertiary volcanic rocks of Nash area in the east of Roudbar, North of Iran. , *Journal of Petrology* 4(15): 39-54 (in Persian).

Hakimi Asiabar S, Bagheriyan S (2018) Exhumation of the Deylaman fault trend and its effects on the deformation style of the western Alborz belt in Iran. *International Journal of Earth Sciences* 107(2): 539-551.

Hakimi Asiaber S, Pourkermani M, Shahriari S, Ghasemi M, Ghorbani M (2011) Tectonic-sedimentary divisions of western Alborz, *Journal of Basic Sciences*, Islamic Azad University, Science Branch And research.

Harangi S, Downes H, Thirlwall M, Gméling K (2007) Geochemistry, petrogenesis and geodynamic relationships of Miocene calc- alkaline volcanic rocks in the Western Carpathian arc, eastern central Europe. *Journal of Petrology* 48(12): 2261–2287.

Harris C, Erlank AJ (1992) The production of large-volume, low-δ18O rhyolites during the rifting of Africa and Antarctica: The Lebombo Monocline, southern Africa, *Geochimica et Cosmochimica Acta* 56(9): 3561-3570.

Harris NBW, Pearce JA, Tindle AG (1986) Geochemical characteristics of collision-zone magmatism, *Journal of Geological Society Special Publications* 19: 67–81.

Herman J, Spandler C, Hack A, Korsakov AV (2006) Aqueous fluids and hydrous melts in high pressure and ultra- high pressure rocks: Implications for element transfer in subduction zones. *Lithos* 92: 399–417.

Hirayama K, Samimi M, Zahedi M, Hushmandzade A (1966) Geology of the Tarom district, western part (Zanjan area –Northwest Iran) G.S.I. ,Rep8.

Hofmann AW, Jochum KP, Seufert M, White WM (1986) Nb and Pb in oceanic basalts: new constraints on mantle evolution, *Earth and Planetary Science Letters* 79: 33–45.

Hollocher K, Robinson P, Walsh E, Roberts D (2012) Geochemistry of amphibolite-facies volcanics and gabbros of the Støren Nappe in extensions west and southwest of Trondheim, Western Gneiss Region, Norway: a key to correlations and paleotectonic settings. *American Journal of Science* 312(4): 357–416.

Hooper P, Hawkesworth C (1993) Isotopic and geochemical constraints on the origin and evolution of the Columbia River basalt. *Journal of Petrology* 34(6): 1203-1246.

Hosseini Abhithabadi M (1984) 1:100000 geological map of Abhar. Sheet 5862. *Geological Organization of Iran.*

Jiang YH, Jiang SY, Ling HF, Zhou XR, Rui XJ, Yang WZ (2002) Petrology and geochemistry of shoshonitic plutons from the western Kunlun orogenic belt, Xinjiang, northwestern China: implications for granitoid genesis, *Lithos* 63: 165-187.

Kermantsky AA, Vushko NA, Budyanskiy DD (1980) Geochemistry of the rare alkalis in sediments and effusives, *Geochemistry International* 178: 54-72.

Khademian F, Monsef A, Rahgoshai M (2018) Petrology and geochemistry of the Eocene volcanic sequence in the northeast of Zanjan: with a perspective on the magmatism of the active continental boundary in the Alborz-Azerbaijan zone, *Journal of Petrology* 9.

Khalatbari Jafari M (2016) Petrology and geochemistry of volcanic lava northeast of Abhar. Design number 111-94. executor of plan.

Khalatbari Jafari M, Akbari M, Qalamgash J (2015) Geology, lithology and magmatic evolution of Eocene volcanic rocks in the Agh Dagh area, north-east of Abhar, *Khorazmi Geosciences Journal* 2: 33-60.

Kuscu GG, Geneli F (2010) Review of post-collisional volcanism in the Central Anatolian Volcanic Province (Turkey), with special reference to the Tepekoy Volcanic Complex. *International Journal of Earth Sciences* 99(3): 593-621.

Le Bas MJ, Le Maitre RW, Streckeisen A, Zanettin B (1986) A chemical classification of volcanic rocks based on the total alkali–silica diagram, *Journal of Petrology* 27: 745-750.

Le Maitre RW (2002) Igneous Rocks: A Classification and Glossary of Terms: Recommendations of the International Union of Geological Sciences Subcommission on the Systematics of Igneous Rocks. Cambridge: *Cambridge University Press* 208.

Lescuyer JL, Riou R (1976) Geologic de la region de mineh (Azerbaijan) Contribution a l'etude du

volcanisme tertiaire de l'Iran. These de 3eme Cycle Grenoble, 233 p.

Leuthold J, Müntener O, Baumgartner LP, Putlitz B, Chiaradia M (2013) A detailed geochemical study of a shallow arc-related laccolith, the Torres del Paine mafic complex (Patagonia), *Journal of Petrology* 54: 273-303.

Lightfoot PC, Hawkesworth CJ, Sethna SF (1987) Petrogenesis of rhyolites and trachytes from the Deccan Trap: Sr, Nd and Pb isotope and trace element evidence, *Contributions to Mineralogy and Petrology* 95: 44–54.

Litvak VD, Spagnuolo MG, Folguera A, Poma S, Jones RE, Ramos VA (2015) Late Cenozoic calc-alkaline volcanism over the Payenia shallow subduction zone, South-Central Andean back-arc (34° 30′–37° S), Argentina. *Journal of South American Earth Sciences* 64: 365-380.

Liu HQ, Xu YG, Tian W, Zhong YT, Mundil R, Li XH, Yang YH, Luo ZY, Shang Guan SM (2014) Origin of two types of rhyolites in the Tarim Large Igneous Province: Consequences of incubation and melting of a mantle plume, *Lithos* 42 (1): 43–46.

McDermott F, Delfin FG, Defant MJ, Turner S, Maury R (2005) The petrogenesis of magmas from Mt. Bulusan and Mayon in the Bicol arc, the Philippines, *Contributions to Mineralogy and Petrology* 150: 652-670.

Mehmood M, Ciarcia S, Lo Schiavo L, Natale J, Vitale S (2023). Paleogeographic and Tectonic Evolution of the Earliest Wedge-Top Basin in the Southern Apennines: New Insights from the Paleocurrent Analysis of the Cilento Group Deposits (Southern Italy), *Geosciences* 13(8), 238.

Moayed M (1991) Petrographic and petrochemical studies of volcanic-plutonic rocks in Tarom region in connection with copper genesis Master's thesis, Faculty of Science, University of Tabriz, 1-175.

MoinVaziri H (1985) Volcanisme tertiaire et quaternaire en Iran, These d, Etat, Université. Paris-Sud. Orsay.

Nabavi MH (1976) An Introduction to the Geology of Iran, Geological Survey of Iran.

Naderi M, Rashidenjademaran N, Aghazadeh M (2012) Geochemistry, origin and geodynamic environment of Zakir-Sarkheh Dizj intrusive mass, southern slope of Tarem sub-zone, east of Zanjan. *Khwarazmi University Science Journal* 31.

Nakamura N (1974) Determination of REE, Ba, Fe, Mg, Na and K in carbonaceous and ordinary chondrites. *Geochimica et Cosmochimica Acta* 38: 757 – 775.

Natali C, Beccaluva L, Bianchini G, Siena F (2011) Rhyolites associated to Ethiopian CFB: Clues for initial rifting at the Afar plume axis, *Earth and Planetary Science Letters* 312: 59–68.

Nouri F, Azizi H, Golonka J, Asahara Y, Orihashi Y, Yamamoto K (2016) Age and petrogenesis of Na-rich felsic rocks in western Iran: evidence for closure of the southern branch of the Neo-Tethys in the Late Cretaceous. *Tectonophysics* 671:151–172.

Pang KN, Chung SL, Zarrinkoub MH, Khatib MM, Mohammadi SS, Chiu HY, Chu C-H, Lee H-Y, Lo C-H (2013) Eocene-Oligocene post-collisional magmatism in the Lut-Sistan region, eastern Iran: Magma genesis and tectonic implications. *Lithos* 180: 234-251.

Paul SW, Honiat C, Trüssel M, Edwards RL, Spötl C (2020) Exceptional warmth and climate instability occurred in the European Alps during the Last Interglacial period. *Communications Earth and Environment* 1 (1): 57.

Pearce JA (1983) Role of the sub-continental lithosphere in magma genesis at active continental margins, Hawkesworth, C.J. and Norry, M.J., eds. Continental basalts and mantle xenoliths, Nantwich, Cheshire: *Shiva Publications*, pp. 230-249.

Pearce JA (2008) Geochemical fingerprinting of oceanic basalts with applications to ophiolite classification and the search for Archean oceanic crust, *Lithos* 100: 14–48.

Pearce JA, Harris N, Tindle AG (1984) Trace element discrimination diagrams for the tectonic interpretation of granitic rocks. *Journal of Petrology* 25(4): 956-983.

Pearce JA, Peate D (1995) Tectonic implications of the composition of volcanic arc magmas. *Annual Review of Earth and Planetary Science*s 23: 251–286.

Perfit M, Gust D, Bence AE, Arculus R, Taylor S (1980) Chemical characteristics of island-arc basalts: implications for mantle sources. *Chemical Geology* 30:.227–256.

Qian X, Wang Y, Feng Q, Zi JW, Zhang Y, Chonglakmani C (2016) Petrogenesis and tectonic implication of the Late Triassic post-collisional volcanic rocks in Chiang Khong, NW Thailand, *Lithos* 248: 418-431.

Qian X, Wang Y, Srithai B, Feng Q, Zhang Y, Zi JW, He H (2017) Geochronological and geochemical constraints on the intermediate-acid volcanic rocks along the Chiang Khong–Lampang–Tak igneous zone in NW Thailand and their tectonic implications. *Gondwana Research* 45: 87-99.

Rollinson HR (1993) Using geochemical data: evaluation, presentation, interpretation. New York: Longman Scientific and Technical Limited 113–121.

Rooney TO, Sinha AK, Deering C, Briggs C (2010) A model for the origin of rhyolites from South Mountain, Pennsylvania: Implications for rhyolites associated with large igneous provinces, *Lithosphere* 2: 211–220.

Sabzehei M (1974) Les mélanges ophiolitiques de la. Theses universite de Granoble.

Saccani E (2015) A new method of discriminating different types of post-Archean ophiolitic basalts and their tectonic significance using Th-Nb and Ce-Dy-Yb systematics. *Geoscience Frontiers* 6 (4): 481-501.

Sadri Espushani S, Amel N, Mokhtari MAA (2014) Petrology and geochemistry of acidic volcanic rocks in

the north of Sulaiman Balaghi (southwest of Hashtjin, north of Zanjan), with a perspective on perlite generation. *Petrology, Earth Sciences Quarterly* 21:156-139.

Sarem MN, Abedini MV, Dabiri R, Ansari MR. (2021) Geochemistry and petrogenesis of basic Paleogene volcanic rocks in Alamut region, Alborz mountain, north of Iran. *Earth Sciences Research Journal* 25(2): 237-245.

Saunders AD, Storey M, Kent RW, Norry MJ (1992) Consequences of plume–lithosphere interactions: Storey, B. C., Alabaster, T., and Pankhurst, R.J., eds., Magmatism and the cause of continental breakup, *Geological Society of Special Publication* 68: 41–60.

Schmidt MW, Jagoutz O (2017) The global systematics of primitive arc melts, *Geochemistry, Geophysics, Geosystems* 18: 2817–2854.

Seyed Qaraini A, Mokhtari MA, Kohestani H (2019) Lithology, geochemistry and tectonomagmatic environment of the Zajkan granitoid massif (Taram-Hashtjin subzone, western Qazvin). *Petrology of Isfahan University* 10.

Stocklin J (1968) Structural history and tectonics of Iran, A review. *AAPG Bulletin* 52(7): 1229-1258.

Sun SS, McDonough WF (1989) Chemical and isotopic systematics of oceanic basalts: implications for mantle composition and processes, In: Saunders AD and Norry MJ (eds), Magmatism in ocean basins. *Journal of Geological Society* 42: 313- 345.

Tatsumi Y, Hamilton DL, Nesbitt RW (1986) Chemical characteristics of fluid plase released from a subducted lithosphere and origin of arc magmas: evidence from high pressure experiments and natural rocks. *Journal of Volcanology* 29: 293-310.

Temel A, Gündoğdu M.N, Gourgaud A (1998) Petrological and geochemical characteristics of Cenozoic high-K calc-alkaline volcanism in Konya, Central Anatolia, Turkey, *Journal of Volcanology and Geothermal Research* 85: 327-354.

Temizel İ, Arslan M (2008) Petrology and geochemistry of Tertiary volcanic rocks from the İkizce (Ordu) area, NE Turkey: implications for the evolution of the eastern Pontide paleomagmatic arc, *Journal of Asian Earth Sciences* 31: 439-463.

Wiley PJ, Rutter M (1986) Experimental data on the solidus of peridotite–CO2 with applications to alkaline magmatism and mantle metasomatism EOS Transactions, *American Geophysical Union* 67: 390.

Wiley PJ, Skine T (1982) The formation of mantle phlogopite in subduction zone hybridization. *Journal of Contribution to Mineralogy and Petrology* 79: 375-380.

Xia R, Wang CM, Qing M, Li WL, Carranza EJM, Guo XD, Ge LS, Zeng GZ (2012) Zircon U–Pb dating, geochemistry and Sr–Nd–Pb–Hf–O isotopes for the Nan'getan granodiorites and mafic microgranular enclaves in the East Kunlun Orogen: Record of closure of the Paleo-Tethys. *Lithos* (234-235): 47-60

Xu W, Zhu DC, Wang Q, Weinberg RF, Wang R, Li SM, Zhang LL, Zhao ZD (2019) Constructing the Early Mesozoic Gangdese crust in southern Tibet by hornblende-dominated magmatic differentiation, *Journal of* Petrology 60(3): 515–552.

Xu X, Song S, Su L, Li Z, Niu Y, Allen M B (2015) The 600–580Ma continental rift basalts in North Qilian Shan, northwest China: Links between the Qilian-Qaidam block and SE Australia, and the reconstruction of East Gondwana, *Precambrian Research* 257: 47- 64.

Yang WB, Niu HC, Cheng LR, Shan Q, Li NB (2015) Geochronology, geochemistry and geodynamic implications of the Late Mesozoic volcanic rocks in the southern Great Xing'an Mountains, NE China, *Journal of Asian Earth Sciences* 113: 454-470.

Zarei Sahamieh R (1992) Petrography, petrology, and geochemistry of north Abhar volcanic rocks and the relationship between volcanism in the region and mineralizations. M.Sc. *Thesis, Faculty of Science*, Tarbiat Moallem University.